Weld World (2013) 57:753–791
DOI 10.1007/s40194-013-0066-y

RESEARCH PAPER

IIW guideline for the assessment of weld root fatigue

Wolfgang Fricke

Received: 18 November 2012 / Accepted: 17 May 2013 / Published online: 23 August 2013

Abstract At welded joints, fatigue cracks usually initiate either at the weld toe or the weld root. The latter may be influenced by small defects or other irregularities or even by non-fused root faces forming a slit which acts like a crack. Weld root failure has therefore to be checked for several weld types. Different approaches exist for fatigue assessment, including the rather simple nominal stress approach, local stress approaches and the crack propagation approach which are partly well suited for the assessment of weld root fatigue. However, it is not easy to keep the overview and to decide which approach should be applied in the case in question. For this purpose, the guideline has been established giving an overview of the different approaches with special emphasis on weld roots and discussing their suitability and the limitations. Six typical examples are described where different approaches are applied and in some cases compared with fatigue tests, thus giving insight into the practical application and allowing own judgement.

Keywords Fatigue cracks · Root runs · Fatigue strength · Stress analysis · Crack propagation · Finite element analysis

1 Introduction

It is well known that welded structures subjected to cyclic loading are prone to fatigue. Fatigue cracks initiate at locations with high stress concentration. These are the relatively sharp transitions between the parent and weld metal at the weld toes as well as weld roots, which are frequently characterised by sharp slits with non-fused root faces acting like crack starters.

The situation is often illustrated by the example of a cruciform joint with load-carrying fillet welds, see Fig. 1. Alternatively to cracks initiating from the weld toes, root cracks may start from the ends of the non-welded root faces, separating the weld throat during crack growth. Which crack type dominates depends mainly on the ratio between throat thickness a (including possible penetration) and plate thickness (t), but also on the type of loading, weld shape, misalignment, residual stresses etc.

Toe and root cracks can be distinguished in failure cases by their characteristic appearance. While toe cracks are located in the weld toe line, at least at the beginning, weld root cracks appear on the weld surface after penetrating through the weld material. Figure 2 shows examples of weld toe and root cracks at the fillet weld around a stiffener termination.

Weld root cracks are frequently considered to be more dangerous than weld toe cracks, as their initiation cannot be detected until they have grown through the whole weld thickness. On the other hand, the residual life of the structure after weld fracture can still be long, particularly in cases with stress variation along the weld; the continuous base plate may even remain intact. Nevertheless, an adequate fatigue strength assessment is necessary to ensure the integrity of the structure and to avoid early and unexpected fatigue failures. This is particularly necessary for optimised structures that have welds with minimised dimensions or post-weld treatment. The latter can improve only the weld toe and not the weld root.

There are various approaches to fatigue strength assessment [16] which are applicable not only to weld toe failure but also to weld root failure. The approaches differ mainly in the stress parameters used for the assessment:

- *Nominal stress approach*, based on stress excluding any stress increase due to the structural detail or the weld; in

Doc. IIW-2384, recommended for publication by Commission XIII "Fatigue of Welded Components and Structures"

W. Fricke (✉)
Institute of Ship Structural Design and Analysis, Hamburg University of Technology, Hamburg, Germany
e-mail: w.fricke@tuhh.de

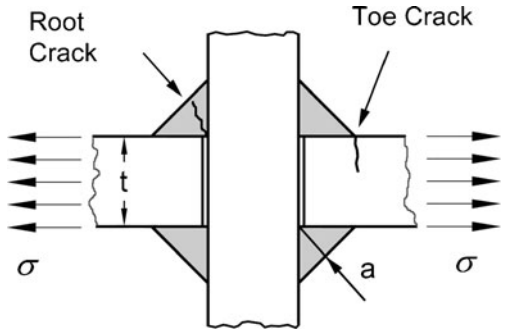

Fig. 1 Possible crack locations in a cruciform joint with load-carrying fillet welds

the case of weld root failure, a nominal stress based on the weld throat thickness has to be used

- *Structural stress approach*, based on stress including stress increase due to structural geometry but excluding that due to local weld geometry; the approach has been developed for weld toe failures but has been extended to some cases with weld root fatigue at fillet welds, using a linearised stress in the weld
- *Effective notch stress approach*, based on local stress at the rounded weld toe or weld root notch, assuming ideal-elastic material behaviour and microstructural support effects to a certain extent
- Approaches based on the *stress intensity factor*, using the *notch stress intensity factor* (N-SIF) of the weld toe with zero radius as the fatigue parameter. For the weld root, the stress intensity factor for crack tips is used
- *Crack propagation approach*, using Paris' law for determining the fatigue life of a propagating crack; while the actual non-fused part is considered as the initial crack at the weld root, an initial crack depth must be assumed for the weld toe

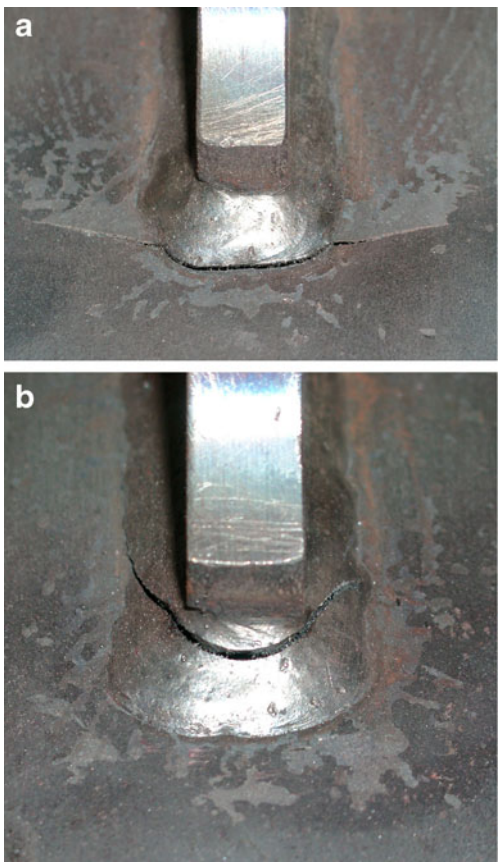

Fig. 2 Weld toe (**a**) and root crack (**b**) at the fillet weld around a stiffener termination

Before the weld root assessment is described and discussed for the different approaches, the scope of applications covered by this guideline is outlined. Finally, several demonstration examples are described, illustrating the range and details of practical application.

Reference is made to several papers, recommendations and guidelines giving more details of the different approaches. It is recommended that different approaches be applied to the actual problem in order to verify the results.

2 Scope of applications

2.1 Butt joints

Typical butt joints with non-fused root faces at risk of weld root fatigue are shown in Fig. 3. In type (a), a two-sided butt weld with embedded root faces, the load-carrying section is reduced to $2 \cdot a$. This case is contained in several catalogues of details in fatigue codes and guidelines, where the stress is to be based on the throat sectional area ($2 \times a$) and a very low fatigue class is assumed. This leads to low fatigue strength so that this detail is not recommended for cyclic loaded structural members.

Non-fused root faces also occur in one-sided butt welds made without a backing bar (i.e. no permanent or ceramic type). In this case, the non-fused root faces can result in early cracks starting from the root. Secondary bending can worsen the situation. This case also typically appears in codes and guidelines, where a very low fatigue class is assumed, particularly in cases where the weld root cannot be checked by appropriate non-destructive testing (NDT).

If, however, the weld root is checked by appropriate NDT and contains rather small axial misalignment, the fatigue strength can be higher [25]. This is utilised in the design of pipelines by defining appropriate measures (NDT, low misalignment) and allowing significantly higher fatigue classes [8, 16].

2.2 Fillet welds

Figure 4 shows different types of cruciform joints with non-fused root faces. Types (a) and (b) are double bevel butt

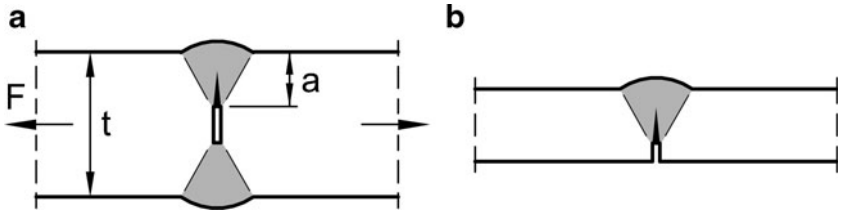

Fig. 3 Butt joints with non-fused root faces at risk of weld root fatigue (cracks indicated)

welds and two-side fillet welds without penetration. Here, the throat thickness *a* determines the weld stress and thus the risk of root fatigue. The depth *e* of the penetration (excluding possible root defects) increases the load-carrying section and hence the fatigue strength. Corresponding fatigue classes can be found in codes and guidelines (e.g. [16]).

The necessary weld throat thickness *a* or leg length *c* to avoid fractures initiating at the weld root can be determined from the fatigue classes based on fatigue tests or from fatigue assessment procedures described in the following section. A typical example for cruciform steel joints with partial penetration welds under axial loading is given in Fig. 5, showing limit curves separating geometries leading to fatigue fractures initiating at the weld toe and root, respectively, derived from fatigue tests. An increased leg length ratio *c*/*b* avoids weld root failures.

The one-sided welds (types (c) and (d) in Fig. 4) are less fatigue-resistant because the weld throat is subjected to additional bending in the case of axially loaded plates. Usually, such welds are only acceptable if weld bending is kept under control, e.g. by transverse stiffening plates. Also, circular or small rectangular hollow sections can provide sufficient restraint, allowing fatigue classes to be based on nominal axial stress only [16].

The welded joints are frequently subjected to loads varying along the weld line which may be due to the geometrical configuration. A typical case is the fillet-welded end of a loaded stiffener where a stress concentration normally occurs and the non-fused root faces terminate (Fig. 6). This requires a local stress analysis and corresponding fatigue assessment.

2.3 Other welds

Special welding processes create connections with limited penetration so that non-welded slits occur. Examples are spot-welds, laser-stake welds and one-sided laser welds, e.g. at T-joints, see Fig. 7. Fatigue cracks may occur at the ends of the slits, separating either the weld or parent metal depending on the loading condition.

The situation is similar to butt and fillet welds with partial penetration, so that the same approaches for fatigue assessment can be applied. One major difference is the loading, which is frequently dominated by shear forces in the connected planes. Thus, special internal forces and moments

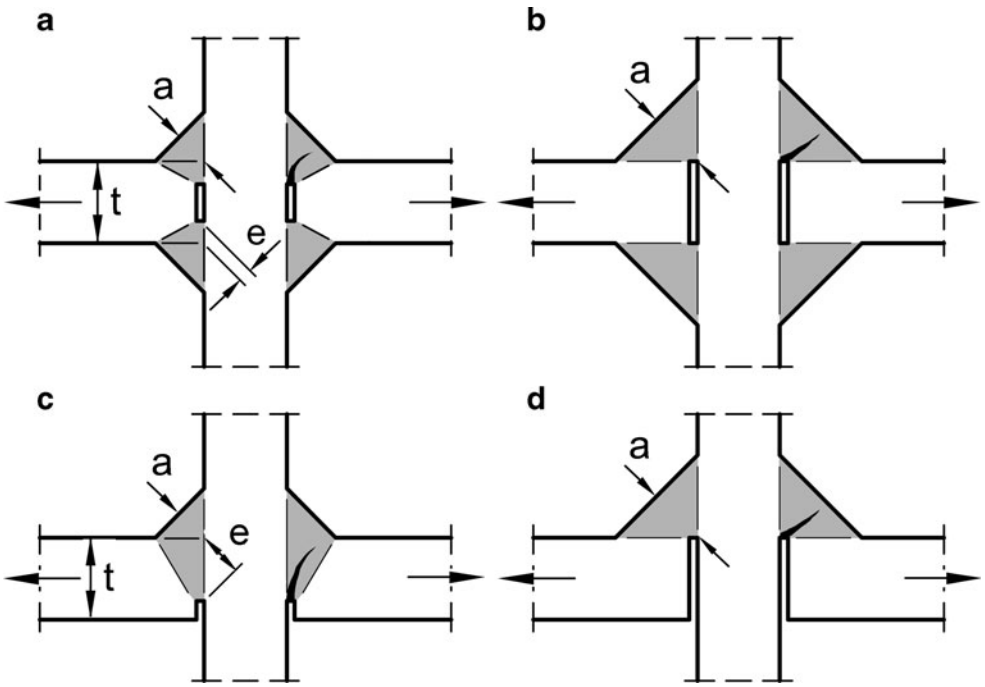

Fig. 4 Fillet welds with non-fused root faces at risk of weld root fatigue (cracks indicated)

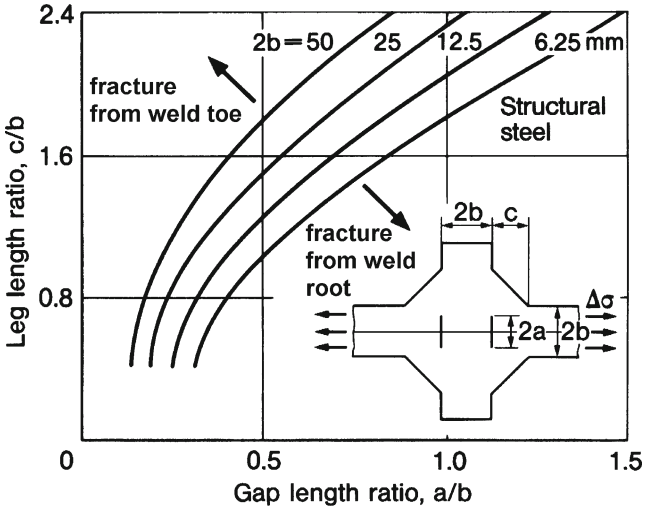

Fig. 5 Limit curves separating fracture from weld toe and root in cruciform joints [24]

are defined in some cases, resulting in specific nominal and/or structural stresses [31].

3 Procedures for fatigue assessment

3.1 General aspects

3.1.1 General procedures

The fatigue assessment procedure can be based on

- S–N curve showing the relationship between the fatigue life in terms of constant amplitude load cycles and a stress parameter, which may be the range of a nominal or local stress in the weld or a stress intensity at a notch. Variable amplitude stresses are taken into account using a damage accumulation hypothesis, normally the linear Palmgren–Miner rule (or Miner's rule).
- Crack growth curve established with a crack propagation law such as the Paris–Erdogan law, based on fracture mechanics and assuming an initial crack length and appropriate material parameters for the analysis. Variable load amplitudes can be considered by an incremental analysis using single load cycles or blocks with different load amplitudes.

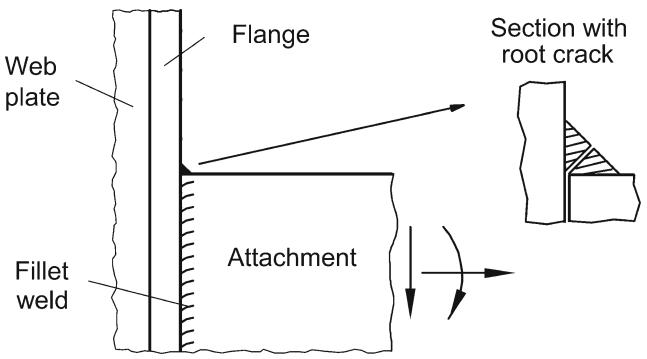

Fig. 6 Fillet-welded end of a loaded stiffener

Further information is given, e.g. by Hobbacher [16] and by several textbooks on fatigue. The following sub-chapters outline the approaches using different stress parameters as well as the approach for crack propagation. The approaches are generally affected by several influence parameters; some of those relevant to root cracking are discussed in general below.

3.1.2 Residual stress

It is well known that residual stresses significantly influence fatigue behaviour [34]. High tensile residual stresses reduce fatigue life, while compressive residual stresses increase fatigue life provided the load ratio is not too high. Crack initiation as well as crack propagation is influenced, the latter mainly by crack closure.

At weld toes, it is usually assumed that unfavourable residual stresses due to welding are present which may reach the yield stress of the material. Therefore, test results for a high stress ratio (R=0.5) are conservatively assumed for any loading [16]. However, weld toes at stiffener ends (Fig. 6) may also show compressive residual stresses because of welding [11].

Welding residual stresses are difficult to measure at the weld root. However, simulations of fillet and butt welds have shown compressive residual stresses at the weld root at a magnitude of the yield strength of the base material in mild strength steels for multi-pass welds [3]. Barsoum [4] also showed that the residual stresses at the weld root side depend on weld penetration and the number of weld passes, where increased compressive residual stresses were observed with increasing weld penetration and an increasing number of weld passes. However, the final residual stress at the weld root side for multi-pass welding also depends on the inter-pass time.

It has been observed that the crack initiation points at pipe-to-pipe connections depend to a great extent on the residual stress state being affected by the welding sequence.

As an unfavourable global residual stress state may be present because of the fabrication and erection of the whole structure, high residual stresses should be assumed also for the weld root unless more favourable conditions are proven. This is usually considered in fatigue strength assumptions in codes and guidelines.

3.1.3 Misalignment

Another factor affecting fatigue strength is misalignment, creating secondary bending stresses which have to be considered in all local approaches, including the crack propagation approach.

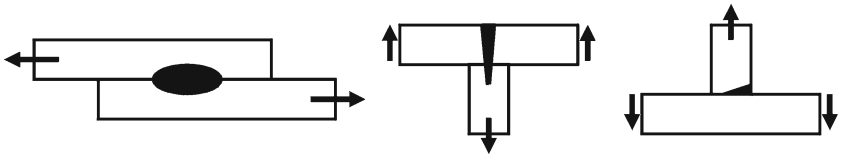

Fig. 7 Other welds susceptible to weld root fatigue

Misalignment effects are particularly large in welds at plates subjected to loading transverse to the weld. For instance, the axial misalignment e of an unrestrained cruciform joint (Fig. 8) creates an increase of the axial stress at the weld toe, which can be expressed by the following stress magnification factor k_m:

$$k_m = 1 + 3e\Big/t \tag{3.1}$$

The secondary bending stress is considerably reduced at the weld root, which has been investigated by Andrews [1]. He derived the following formula for the stress magnification at the weld root:

$$k_m = 1 + e\Big/(t+h) = 1 + e\Big/\left(t + a\sqrt{2}\right) \tag{3.2}$$

The right part applies to fillet welds with 45° flank angle. Other cases such as angular misalignment may be analysed by simple beam theory. Additional restraint in the weld direction, e.g. by stiffeners or curved shell effects, may require a 3D finite element analysis.

3.2 Nominal stress approach

3.2.1 Overview of the approach

The nominal stress approach uses for fatigue assessment a stress which disregards the local stress increase due to structural discontinuity (e.g. a stiffener termination) and also due to the local weld profile. These effects are included in notch cases containing structural details which are associated with design S-N curves allowing the fatigue life to be assessed (also called FAT classes).

In the case of weld root fatigue, a nominal stress in the weld is used. This might require a special analysis which is outlined below. As already mentioned in Section 2, several notch cases are defined in codes and guidelines for different types of joints (e.g. [16]). The associated fatigue class is relatively low (FAT 36–40), defining the characteristic fatigue strength of the design S–N curve at two million cycles for a survival probability of 97.7 %. The reasons for the low fatigue class are that a very sharp notch is present and that the nominal stress in the weld disregards any local bending effects.

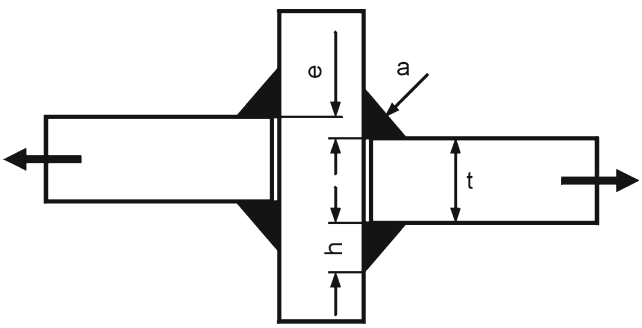

Fig. 8 Axial misalignment e of a cruciform joint

In general, the nominal stress approach is the easiest to apply, requiring only a simplified stress determination. Several influence factors such as misalignment effects are implicitly taken into account to a certain extent, whereas others, such as weld throat bending, are neglected or only roughly considered. The nominal stress approach should thus be applied only to the cases and within the limits defined by the notch cases described in codes and recommendations.

3.2.2 Nominal weld stress

Nominal stress is often determined by formulas using load parameters, such as forces and bending moments, as well as section properties, such as section area and modulus. Alternatively, relatively coarse finite element models are used. It should be borne in mind that stress raisers which are not typical of the welded detail itself must also be taken into account (e.g. reduced effective widths).

In *butt joints*, the nominal weld stress can often be calculated directly from the nominal stress in the adjacent plate, taking into account any reduced sectional area, see Fig. 3. Weld reinforcement is usually neglected.

In *fillet welds*, a special weld stress is usually applied, illustrated in Fig. 9a by a cruciform joint with fillet welds. The weld stress $\sigma_{n,w}$ is based on averaged stress components in the weld throat which are also used in the static design of welds, i.e.

- The stress $\sigma_\perp$ normal to the weld throat section
- The shear stress $\tau_\perp$ in the weld throat section

As illustrated in Fig. 9b, c, the horizontal or vertical leg sections, reduced to the throat thickness a, may also be considered to determine the averaged stress components $\sigma_\perp$ and $\tau_\perp$.

The stress components are combined by vector addition into the nominal weld stress $\sigma_{n,w}$, i.e.

$$\sigma_{n,w} = \sqrt{\sigma_\perp^2 + \tau_\perp^2} \tag{3.3}$$

In simple cases, the stress components can be determined by equilibrium conditions from the nominal stress σ_n in the

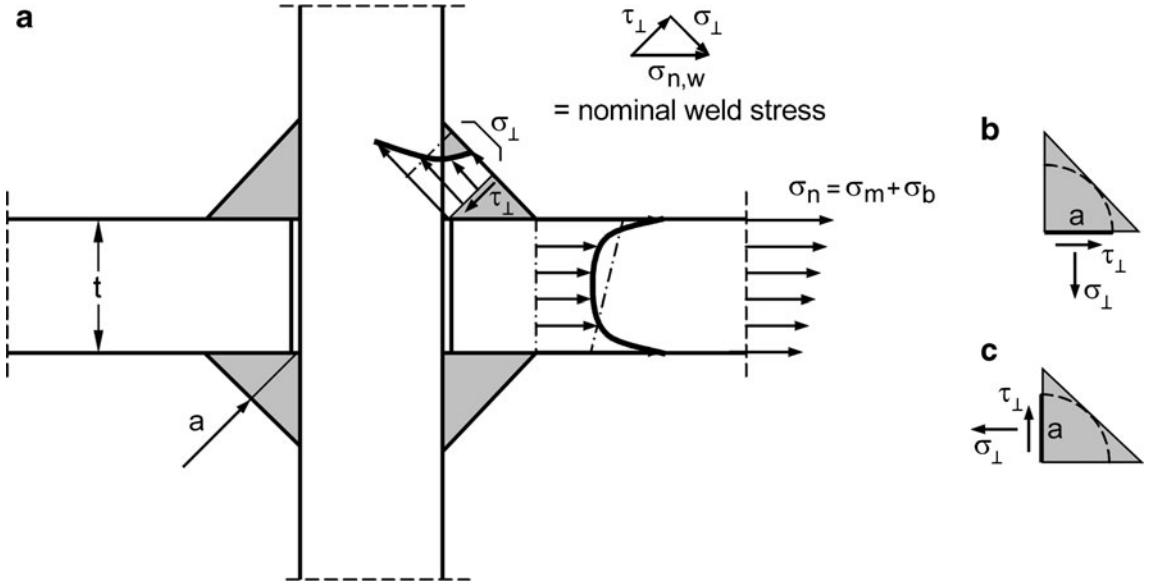

Fig. 9 Fillet-welded cruciform joint with nominal stresses in plate and weld

plate or, in more complex cases, by the finite element method using the forces or stresses in the weld.

In the case of the cruciform joint, the nominal weld stress can also be determined by simply referring the axial force in the plate ($\sigma_m \times t$) to the weld throat area ($2a$) and the bending moment ($\sigma_b \times t^2/6$) to the weld throat area multiplied by the distance between the weld legs ($a \times t$):

$$\sigma_{n,w} = \sigma_m \frac{t}{2a} + \sigma_b \frac{t}{6a} \tag{3.4}$$

Other cases can be treated analogously. Special cases are one-sided fillet and partial penetration Y-butt welds, where the secondary bending stress is casually considered in the nominal weld stress in connection with an increased fatigue class. The stress is frequently regarded as a structural stress, see Section 3.3.

3.2.3 Notch cases

Codes and guidelines based on the nominal stress approach usually contain several notch cases for weld root fatigue. Section 2 summarises such cases without stating all details.

The related fatigue classes according to the IIW Fatigue Design Recommendations [16] may be grouped according to the following principles:

- *Butt joints* made from *one side with weld root controlled* by a backing bar or NDT are classified as FAT 71–80 for steel and FAT 25–28 for aluminium.
- If *butt joints* contain *embedded non-fused root faces* and/or if the *weld root cannot be controlled* by NDT, the joint is classified as FAT 36 (steel) or FAT 12 (aluminium).
- *Fillet welds and partial penetration K-butt welds* are classified as FAT 36 (steel) or FAT 12 (aluminium). Relatively thin fillet welds ($a/t \leq 1/3$) are assessed one class higher. Exceptions are one-sided fillet and partial penetration Y-butt welds if the secondary bending stress is included (leading to FAT 71 for steel and FAT 25 for aluminium). Welds connecting the end of a hollow section are classified as FAT 36–45 for steel and FAT 14–16 for aluminium (depending on section shape and thickness)
- Special cases are *butt-welds of three-plate joints* and *fillet welds at lap joints*. Here, the non-fused root faces are parallel to the loading direction. In the case of butt-welds, FAT 63–71 applies to steel and FAT 22 to aluminium. Double lap joints are classified as FAT 45 for steel and FAT 16 for aluminium, whereas overlap joints are downgraded to FAT 36 (steel) and FAT 12 (aluminium) due to the additional throat bending.

3.2.4 Multiaxial loading

Further stress components may be acting in addition to those shown in Fig. 9. The shear stress τ_{II} parallel to the weld line is primarily relevant to fatigue. The interaction equation according to Gough—Pollard, which corresponds to the von Mises hypothesis, can be used to describe the combined effect of stress components, i.e. $\sigma_{n,w}$ and $\tau_\parallel$ in this case:

$$\left(\frac{\sigma_{n,w}}{FAT(\sigma,N)}\right)^2 + \left(\frac{\tau_\parallel}{FAT(\tau,N)}\right)^2 \leq D_{MA} \tag{3.5}$$

with the multiaxial damage parameter $D_{MA}=1$ and the particular fatigue strengths (FAT) for normal and shear stresses at the anticipated number of load cycles N, see Sonsino and Wiebesiek [39], Hobbacher [16], Wiebesiek and Sonsino [45], Sonsino [36] and Sonsino [37].

If the normal stress component parallel to the weld $\sigma_{\parallel}$ is to be considered too, then this has to be done by deriving either the principal stress or the von Mises stress from $\sigma_{n,w}$ and $\sigma_{\parallel}$, but without the shear stress component $\tau_{\perp}$.

A further alternative for the case of proportional stress components, an extension of Eq. (3.3), has been proposed [23], using the averaged parallel shear stress in the weld throat $\tau_{\parallel}$:

$$\sigma_{n,w} = \sqrt{\sigma_{\perp}^2 + \tau_{\perp}^2 + 0.2 \cdot \tau_{\parallel}^2} \tag{3.6}$$

The above proposed Eq. (3.5) results in acceptable evaluations for proportional loading with constant principal stress directions. However, in the case of non-proportional loading with changing principal stress directions, these equations, including Eq. (3.3), fail because they do not display the fatigue life reduction for ductile materials and overestimate fatigue life significantly, i.e. the calculations are on the unsafe side. For this, a modification of the Gough–Pollard Eq. (3.5) by the multiaxial damage parameter D_{MA}=0.5 is suggested, rendering good assessments, see Sonsino and Wiebesiek [39], Wiebesiek and Sonsino [45], Sonsino [36] and Sonsino [37].

3.3 Structural stress approaches

3.3.1 Overview of the approaches

In contrast to nominal stress, *structural stress* contains the stress increase due to the structural configuration, e.g. caused by the *structure-related stress concentration* or additional *plate bending* including significant misalignment effects. Not considered is the local stress peak by the weld itself because of its sharp notches at the weld toe and root.

At *weld toes*, structural stress is usually determined by extrapolating the surface stress to the hot-spot, termed *structural hot-spot stress* [30]. Another way of omitting the local stress peak is stress linearisation in the thickness direction.

Surface stress extrapolation is not suitable for the fatigue assessment of weld roots. Therefore, approaches exist which utilise *local nominal stress* or *structural weld stress* derived from the forces and moments or from the stress distribution in the weld itself, partly restricted to definite cases of application. Figure 10 gives an overview of the different approaches together with the stress types used and the FAT classes for steel. The approaches are briefly described in the following.

In contrast to the nominal stress approach, the structural stress approach for weld root fatigue offers the possibility of considering explicitly the stress increase in a weld because of local structural stress concentrations and/or local weld throat bending caused by geometrical configuration or misalignment effects. Here, the approach offers advantages over the nominal stress approach, though it is still based on rather simple analysis models. This implies on the other hand the assumption of a simplified stress distribution in the weld throat by averaging or linearising it. The approach has been verified by several examples which define and limit its scope of application.

3.3.2 Approach for fillet-welded attachment ends

In fillet welds around loaded attachment ends, as illustrated in Fig. 6, increased stresses occur due to the concentrated

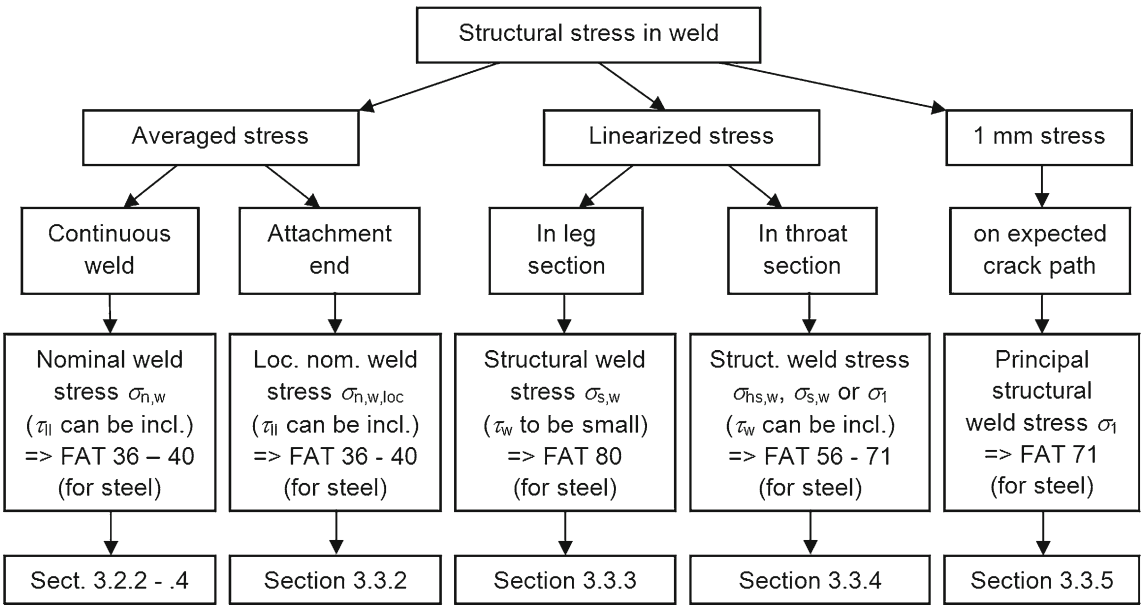

Fig. 10 Overview of the different structural stress approaches for weld root fatigue assessment

force flow in the corner. The increased stress averaged in the weld throat area around the attachment end can be estimated from the transmitted force F_e as outlined in Fig. 11 [13] while the local weld throat bending is neglected. This stress can be considered as *structural weld stress* or *local nominal weld stress*, averaged over a definite area.

One must distinguish between two cases. In the *first case*, the plate stress σ_p in the attachment is acting perpendicular to the fillet weld (Fig. 11) without any other significant stress component such as a shear stress parallel to the weld. Weld root failure is caused by the stress transferred through a fillet weld with throat thickness a.

It is assumed that the force F_e at the end of the attachment, representing the local plate stress σ_p in a reference area up to $t/2$ from the attachment end (t=plate thickness), is transferred through the hatched effective weld area in Fig. 11 (section A–A). The averaged local nominal weld stress $\sigma_{n,w,loc}$ in this effective weld area due to this force F_e becomes:

$$\sigma_{n,w,loc} = \frac{F_e}{2a \times t + a^2} \tag{3.7}$$

Here, the weld area is conservatively assumed to have throat thickness a (not leg length). It has been shown that the stress intensity factors of this complex 3D situation at attachment ends and of the corresponding 2D case of cruciform joints are almost the same [13]. As a consequence, the fatigue assessment can be based on the same fatigue class as for cruciform joints (FAT 36–40 for steel).

The local nominal or structural weld stress can be determined from a finite element model with shell or solid elements in the attachment having a breadth of $t/2$ or even t. Their stresses are used to derive the force F_e from the averaged local plate stress $\sigma_{n,p,loc}$ in the reference area $t \times t/2$. As an alternative, the local nominal weld stress may be determined directly in the section A–A, where the normal stress components can be evaluated from selected weld elements of a finite element model. It should be mentioned that the load transmitted has to be referred to the effective weld area shown in Fig. 11. If the non-fused slit is modelled, nodal forces rather than element stresses should be evaluated in coarse finite element meshes [13]. However, the evaluation of the loads transmitted is also possible when the slit is not modelled.

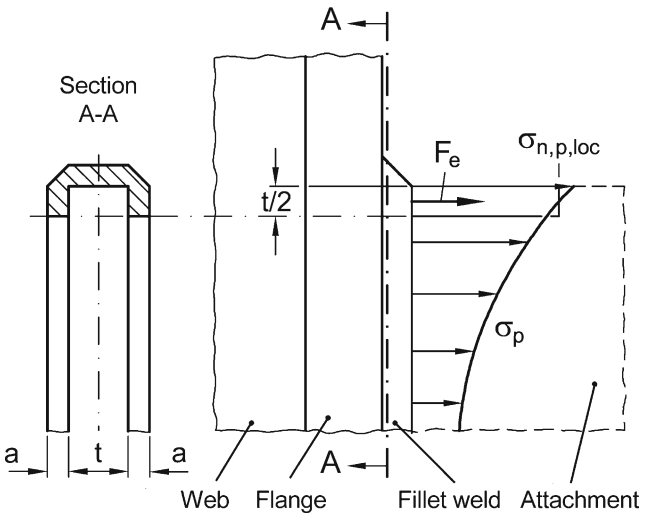

Fig. 11 Geometry and loading of the end of an attachment similar to that in Fig. 6

In the *second case*, not only are there normal stresses acting perpendicular to the weld, as assumed in Fig. 11, but also significant shear stresses acting parallel to the weld. These are present particularly in attachment ends with soft toes, where weld root failures may also occur.

Two possibilities for their consideration have been proposed. In the first, the averaged stress components in the effective weld area are used, i.e. normal stress $\sigma_\perp$ and parallel shear stress $\tau_\parallel$, see Fig. 12a. They can be evaluated in the same way as described above. The following equivalent weld stress has been proposed for the fatigue assessment:

$$\sigma_{n,w,loc} = \sqrt{\sigma_\perp^2 + \tau_\parallel^2} \tag{3.8}$$

The alternative approach uses the resultant force F_e at the attachment end acting in the reference area $t \times t/2$ in the plate next to the weld. This force and its angle φ from the normal may be derived from the averaged principal stresses at the nodal points in the reference area. It is assumed that the total force F_e is transferred through the effective weld area, reduced according to the angle φ, see Fig. 12b. Then the resulting local nominal stress in the weld becomes:

$$\sigma_{n,w,loc} = \frac{F_e}{2a\left(t - a\sqrt{2}\tan\varphi\right) + a^2} \text{ with } \varphi \le \arctan\left(\frac{t}{2a\sqrt{2}}\right) \tag{3.9}$$

The averaged principal stress $\sigma_{1,n,loc}$ acts on the projection of the reference area $t \times t/2$, which is considered as follows when calculating the force F_e:

$$F_e = \sigma_{1,n,loc} \times \left(t^2/2\right) \times \cos\varphi \tag{3.10}$$

As shown in Eq. (3.9), the evaluation is no longer valid for large angles φ, which may occur when the reference area

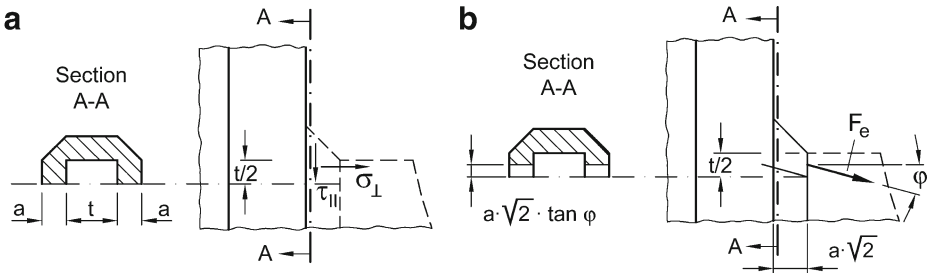

Fig. 12 Consideration of horizontal shear stresses using **a** stress components in the weld and **b** the force F_e derived from the local principal plate stress in the attachment

for stress evaluation comes too close to the upper surface of the soft toe.

An application of the approach is demonstrated in Section 4.2.

3.3.3 Approach for local weld throat bending using stresses in the weld leg

Local weld throat bending occurs particularly in one-sided fillet or partial-penetration welds (see Fig. 4c, d) and is caused by eccentric load transfer or bending of the attached plate. Fricke et al. [15] presented an approach for the fatigue assessment of fillet welds which are predominantly subjected to throat bending. They proposed using the linearised stress in the leg plane in the extension of the root face (section A–A in Fig. 13a), and not in the weld throat, because fatigue tests as well as crack propagation analyses at cruciform and hollow section joints had shown that the crack path was closer to this plane than to the weld throat section. In addition, the stress in the leg section—in contrast to that in the throat section—is characterised in several cases mainly by normal stresses (i.e. axial and bending stress, $\sigma_{m,w}$ and $\sigma_{b,w}$, respectively) and less by shear stresses τ_w. This facilitates the stress analysis and even allows the evaluation of linearised stresses in one-sided welds from the loads in the attached plate by equilibrium conditions as outlined below. The leg length should be limited to the thickness of the attached plate to avoid non-conservative results.

If mainly axial and bending stresses are acting and shear stresses are small, fatigue class FAT 80 has been found from different fatigue test series to be appropriate for welds of steel. The fatigue class is higher than that mentioned in the previous sub-section because the bending portion is now included. It should be noted that larger shear stresses τ_w change the direction of the principal stress and, hence, the crack path. If in doubt, the amount of τ_w and the applicability of the approach should be checked (it has been proposed that it should be less than 20 % of the normal stress, which changes the principal stress direction by about 10°).

Using finite element models with solid elements The stresses or forces in the leg section can be directly linearised to obtain the membrane and bending portion $\sigma_{m,w}$ and $\sigma_{b,w}$, respectively, of the structural weld stress $\sigma_{s,w}$:

$$\sigma_{s,w} = \sigma_{m,w} + \sigma_{b,w} \tag{3.11}$$

$$\sigma_{m,w} = \frac{1}{\ell}\int_0^{\ell} \sigma(z)\mathrm{d}z \tag{3.12}$$

$$\sigma_{b,w} = \frac{6}{\ell^2}\int_0^{\ell} \sigma(z)\left(\frac{\ell}{2} - z\right)\mathrm{d}z \tag{3.13}$$

where $\sigma(z)$ is the stress normal to the leg section, z the coordinate along the weld leg and ℓ the leg length, see Fig. 13a. In the same way, the shear stresses τ_w can also be linearised.

The determination of structural weld stresses from finite element models can become unreliable due to the influence of the notch singularity at the weld root [14]. Therefore it is recommended that internal nodal forces be used instead of element stresses for the integration according to Eqs. (3.12) and (3.13), as these naturally satisfy equilibrium conditions.

If a one-sided weld is present, as shown in Fig. 13a, the structural weld stress can also generally be derived from the membrane and bending portion σ_m and σ_b of the structural stress in the attached plate by using equilibrium conditions between the weld and the plate sections. This means that a relatively coarse mesh established for the analysis of structural hot-spot stresses can be used.

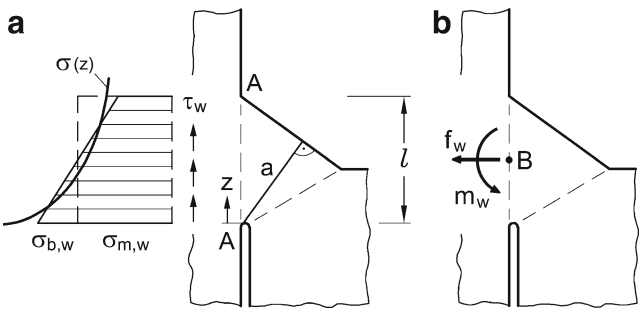

Fig. 13 Linearisation of stresses in the leg section A–A of the weld (**a**) and internal normal force and moment per unit length in leg section (**b**)

An application of this approach is demonstrated in Section 4.3.

Using finite elements models with shell elements In a *model with shell elements*, the structural stress components can be directly obtained from the internal forces and moments f_w and m_w per unit length acting at the weld leg mid-line, see Fig. 13b, by the following equations:

$$\sigma_{m,w} = \frac{f_w}{\ell} \tag{3.14}$$

$$\sigma_{b,w} = \frac{6\, m_w}{\ell^2} \tag{3.15}$$

f_w and m_w can also be obtained from an appropriate shell element model such as the one described for a one-sided weld by Turlier et al. [42]. Element nodes are located at mid-height of the leg section (point B). The internal forces and moments are obtained by transformation of nodal forces using the shell element shape functions. Metal sheets are represented by their mid-surfaces, meshed with shell elements. In order to assess fatigue, node locations are forced at the root and the toes, see Fig. 14a.

The weld is represented by shell elements which are connected to the sheets using the FEA gluing technique. Weld leg nodes are projected on the mid-surfaces and linked with rigid body elements. Finally, the projected nodes are coupled with sheet element nodes using multipoint constraints.

With weld throat thickness assigned as the shell thickness and the gluing technique avoiding additional rigidity, the model is representative regarding the stiffness of the assembly, see Fig. 14b. Moreover, local nominal weld stress can be determined by extracting the loads on the shell element. The shear stress component is obtained if thick shell element formulation is used.

The approach is applied to different examples in Section 4.

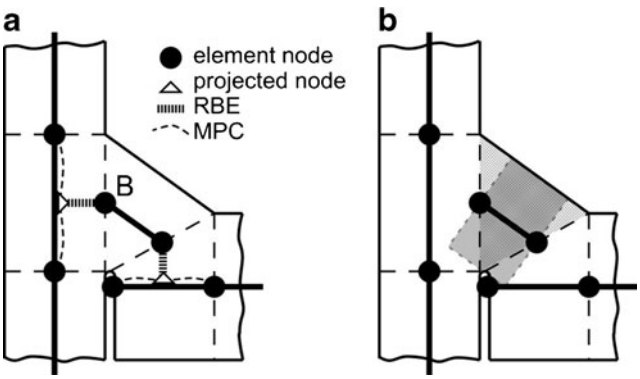

Fig. 14 Shell element model (**a**) and equivalent section (**b**)

3.3.4 Approaches for local weld throat bending using stresses in the weld throat

A specific procedure for the fatigue assessment of weld root failure using stresses in the weld throat has been proposed by Sørensen et al. [40], allowing various load combinations to be considered. The weld is modelled by isoparametric 20-node hexahedronal elements such that two elements describe the throat section line, see Fig. 15. Linear elements would require a finer mesh.

The structural stress evaluation is based on an extrapolation of the stresses evaluated at two points located one quarter of the throat thickness apart from the weld root or weld surface respectively. The stresses at these 'quarter points' are linearly extrapolated to the weld root, where a stress singularity exists, thus defining the 'hot-spot weld stress' $\sigma_{hs,w}$. The authors showed that in several cases it was sufficient to evaluate and extrapolate the first principal stress σ_1 at the mid-side nodes of the two elements. In more complex load cases, the recommendation is to extrapolate the six stress components σ_x, σ_y, σ_z, τ_{xy}, τ_{yz}, and τ_{zx} to the weld root and then to evaluate the first principal stress there. Specific meshing rules have to be observed in the neighbourhood of the weld.

The hot-spot weld stress was successfully used to describe a uniform narrow scatter band of fatigue test results for fillet-welded cover plates and cruciform specimens made of structural steel, comprising different degrees of weld throat bending. An evaluation with the prescribed inverse slope exponent m=3 results in a characteristic fatigue strength of 61 N/mm^2 based, however, on a probability of survival P_s=95 %.

A similar approach was proposed by Hong [17] using the axial and bending stress in the weld throat in connection with the same stress parameter used in previous proposals for the weld toe, thus considering effects of thickness and stress gradient. A similar approach has been applied to the ends of longitudinal attachments by Maddox et al. [26]. In order to fit Maddox's test results with fatigue strength of

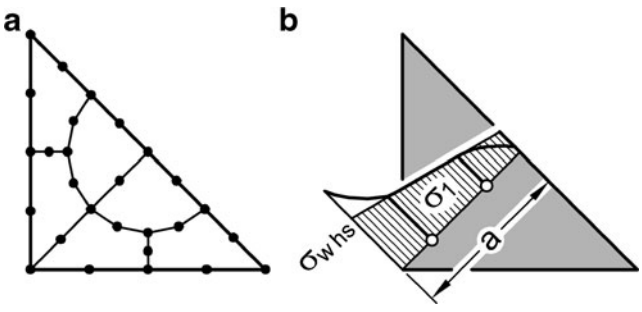

Fig. 15 Fillet weld modelling by 20-node hexahedronal elements and evaluation of the hot-spot weld stress by linear extrapolation (after [40])

FAT 80, the idea is to transpose the linearised structural stress calculation as described in Section 3.3.2 to any section through the weld throat. Turlier et al. [43] have developed an analytical formula based on weld leg line forces and moments and weld throat sizes. It gives the structural stress at the weld root depending on the angle of the weld throat section. The maximum structural stress may be evaluated. This has been also used in the case of asymmetric fillet welds subject to pure bending. In special cases, the stress in the plate adjacent to the weld may additionally have to be taken into account, particularly in the case of high penetration joints [43].

3.3.5 Approach using the 1-mm stress

Xiao and Yamada [48] proposed applying their structural stress approach using the 1-mm stress not only to weld toes, but also to weld roots. The idea behind the approach is that the stress at a distance of approx. 1 mm from the local notch in the direction of the expected crack propagation is representative of the early crack propagation phase which accounts for the major part of the fatigue life.

The approach has successfully been applied to various fillet-welded joints with weld toe failure, resulting in characteristic fatigue strength of FAT 100. The application to cruciform joints with weld root failure indicated a fatigue class reduced to approx. FAT 71.

The stress analysis requires a relatively fine finite element mesh with elements having a size of max 1 mm (better 0.5 mm), allowing stress evaluation at the nodal point at a distance of 1 mm from the weld root. It is not fully clear which stress component should be used for the fatigue assessment. In case of doubt, the first principal stress should be evaluated conservatively.

3.4 Effective notch stress approach

3.4.1 Overview of the approach

The *effective notch stress approach* considers the increase in local stress at the notch formed by the weld toe or the weld root, based on theory of elasticity, i.e. without consideration of elastic–plastic material behaviour. The micro-structural support effect of the material, which considers the effect on fatigue behaviour of the inhomogeneous material structure under a stress gradient, may be taken into account by averaging the stress over a definite area.

This approach is mainly used in the form of fictitious notch rounding, see Fig. 16 [12, 16, 31]. The basic idea behind this approach is that the stress reduction in a notch due to averaging the stress over a certain depth can alternatively be achieved by a fictitious enlargement of the notch radius ρ_f.

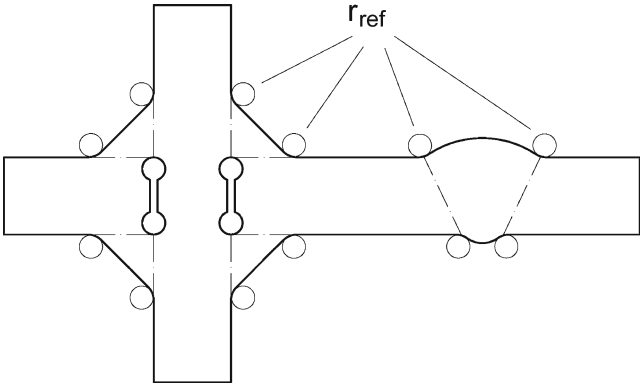

Fig. 16 Fictitious notch rounding (graph according to [16])

In a ‘worst case’ or conservative way, Radaj assumed a fictitious radius of r_{ref}=1 mm, meanwhile termed *reference radius*. This reference radius derived for welded joints in steel is also used for welded joints in aluminium and magnesium alloys.

The notch rounding with a reference radius of 1 mm may cause problems in thin structures less than 5 mm thick. In particular, the groove created by this radius at the weld root causes a substantial reduction in cross-section and hence modifies the stress distribution, which affects the results of the fatigue assessment.

Therefore, a *small-size notch approach* which uses a reference radius r_{ref}=0.05 mm has been proposed for assessing root failure of welded joints in thin-sheet material (steel, aluminium and magnesium alloys) in particular. The re-evaluation of tests shows that it seems to be better suited also to the fatigue assessment of relatively thick laser stake-welded T-joints if the slope exponent m=3 is assumed for the S–N curve [10].

The main advantage of the effective notch stress approach over the nominal and structural stress approaches is that the local stress in the relevant notch is explicitly taken into account so that influencing factors like the actual local geometry including weld throat thickness and the local stress distribution etc. are considered. However, the weld geometry still has to be idealised, particularly at the weld root, so that irregularities and other effects such as residual stresses can only be considered by the S–N curve chosen.

3.4.2 Modelling and numerical analysis

The rounding of the roots of non-penetrating fillet welds is shown in Fig. 16. The length of the non-welded root faces is retained by locating the vertex point of the circle at the weld root, see Figs. 17 and 18. Different shapes are possible [32], among others the keyhole notch and the U-shaped notch, Fig. 17b, c. The latter reduces the high stress concentration in the keyhole notch for loading parallel to the non-welded root faces, but it should be noted that it can also lead to an

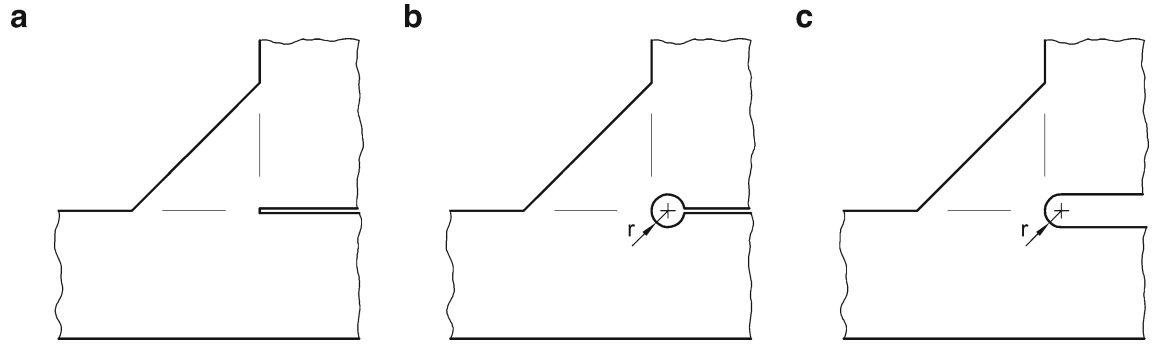

Fig. 17 Rounding of the weld root of a non-penetrating fillet weld by a keyhole and a U-shaped notch

underestimation of the required notch stress for assessing potential fatigue failure in the weld throat. Therefore, it cannot generally be recommended.

In thin-walled structures it might be necessary to compensate for the increase in net section stress due to the notch depth [31].

Usually, notch stress is computed numerically using the finite element method. The stresses may be solved by 3D or a 2D analysis, the latter being restricted to special cases where variations of the geometry and loading in the 3rd direction can be neglected. In this case, plane strain conditions are usually assumed, as biaxial stresses occur in the notches due to restraint in the 3rd direction.

The discretisation of the structure is normally performed such that a relatively coarse overall mesh is established, which is locally refined in the neighbourhood of the notches under consideration. The mesh should be gradually refined towards the notched area, avoiding large steps in element size and excessive element distortion. Figure 19 shows a typical example for a weld root modelled with a keyhole notch.

Recommended element sizes at the notch root rounded with radius r are $r/4$ or less for elements with higher-order displacement functions and accordingly reduced for elements with linear displacement function [12]. It should be observed that this element size applies to the directions along the rounded notch surface as well as those perpendicular to it, in the latter preferably even smaller in size because of the steep stress gradient.

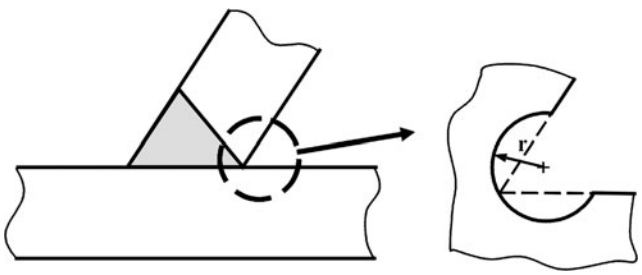

Fig. 18 Notch rounding of the weld root of a Y joint

Notch stresses on the rounded surface of the notch are evaluated, using the tangential and normal stresses in the section and the shear stresses on the notch surface. From these, principal or equivalent stresses can be derived.

Further aspects for modelling and stress evaluation are discussed by Fricke [12].

3.4.3 S–N curves and FAT classes

The FAT classes to be used for the S–N curve in the effective notch stress approach were derived from a statistical analysis of relevant fatigue test results obtained from welded joints and associated notch stress analyses. The results of the analyses are summarised in the left part of Table 1 for the reference radius r_{ref}=1 mm and in the right part for the reference radius r_{ref}=0.05 mm. It should be noted that these fatigue classes have been derived based on the assumption that the S–N curve has a slope exponent of m=3. Different slope exponents, e.g. m=5, have been observed, particularly in thin-walled structures, leading to suggestions for modified approaches [38].

The FAT classes are based on the range of maximum principal stress in the notch root. A reduction by one category is recommended should the equivalent von Mises stress be assessed. This is recommended particularly for cases with predominant shear loading parallel to the weld line, characterised by principal stresses on the notch surface having different signs. Further details have been given, e.g. by Fricke [12] and Sonsino [35].

3.4.4 Multiaxial fatigue

Multiaxial stress states with proportional loading can be assessed using either the range of the maximum principal stress—as long as both principal stresses have the same sign—or the equivalent von Mises stress as described in the previous section. The interaction equation presented in Section 3.2.4 can be used too, using the local stress components and respecting the stated limitations between proportional and non-proportional loading.

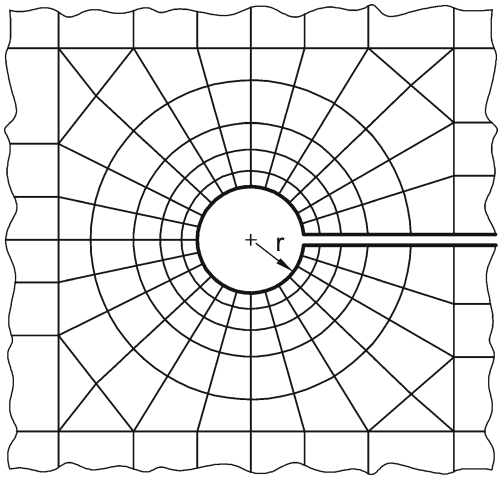

Fig. 19 Typical mesh for a notch stress analysis with elements having a quadratic shape function at a weld root modelled with a keyhole shape

3.5 Approaches based on the stress intensity factor

3.5.1 Overview of the approaches

The theoretically infinite stress at sharp V-notches with notch opening angle 2α can be described by a N-SIF in a similar way as for crack tips. Local stress distributions in plane configurations are given as a combination of a symmetric and skew-symmetric stress field. The N-SIFs K_1 and K_2 for modes I and II loading quantify the magnitude of the asymptotic stress distribution according to the theoretical solution of Williams [46].

The N-SIFs can be used directly to describe the crack initiation at sharp corners [5, 44]. Lazzarin and Tovo [18] developed an N-SIF approach for welded joints and showed that fatigue test results of various welded joints form an S–N curve with reasonable scatter if based on N-SIF.

The N-SIF approach requires knowledge of the elastic stress field in the region very close to the notch tip. In a similar way as for the stress analysis at crack tips, finite element meshes must be very fine in this region.

Table 1 Characteristic fatigue strength (P_s=97.7 %, N=2·10^6) for welds of different materials based on maximum principal stress

Material	Characteristic fatigue strength for r_{ref}=1 mm	Characteristic fatigue strength for r_{ref}=0.05 mm
Steel	FAT 225	FAT 630
Aluminium alloys	FAT 71	FAT 180
Magnesium	FAT 28	FAT 71

However, the N-SIFs K_1 and K_2 can be related to the total elastic *strain energy density* (SED) $\overline{W}$ averaged over a cylindrical sector with a given characteristic radius R_0 in the case of the modes I and II stress distributions under plane strain conditions by the following equation:

$$\overline{W} = \frac{e_1}{E}\left[\frac{K_1}{R_0^{1-\lambda_1}}\right]^2 + \frac{e_2}{E}\left[\frac{K_2}{R_0^{1-\lambda_2}}\right]^2 \tag{3.16}$$

where: E=Young's modulus

λ_1, λ_2 = the eigenvalues of the stress field for K_1 and K_2 modes (see Fig. 20)

e_1, e_2 = parameters depending on the notch opening angle 2α.

When 2α is 135°, a typical value for fillet-welded joints, the mode I stress distribution is singular ($1-\lambda_1$=0.326), whereas the mode II distribution is not ($1-\lambda_2$=-0.302). For 2α=0°, all distributions are singular and reflect the characteristic stress field at a crack tip. The parameters e_1 and e_2 have been described analytically by Lazzarin and Zambardi [19]. For 2α=135°, these are e_1=0.118 and e_2=0.111 and for 2α=0° e_1=0.133 and e_2=0.34.

The control radius R_0 is material-dependent and has been proposed by Lazzarin and Zambardi [19] and Livieri and Lazzarin [22] to be 0.28 mm, considering the failure behaviour of conventional fillet-welded joints under mode I loading for steel. For an opening angle of 0°, this value is conservative. Corresponding considerations would result in R_0=0.36 mm.

The correlation between the average elastic SED and the N-SIF offers a practical way of computing the relevant fatigue parameter with a coarser finite element model. The average SED can be used directly as the fatigue parameter (*SED approach*), which allows the results of different

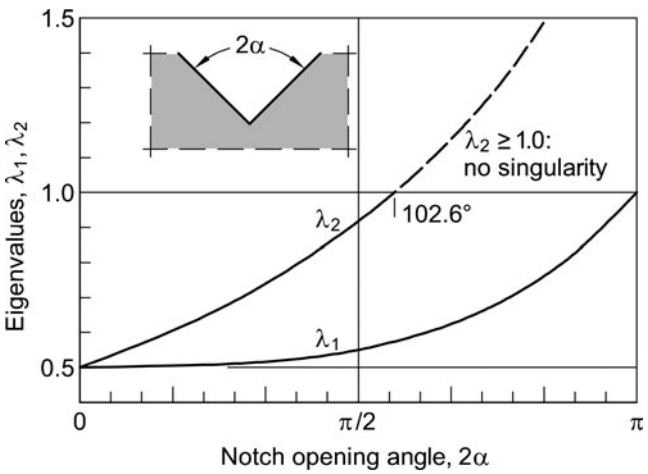

Fig. 20 Eigenvalues defining the order of stress singularity at sharp V notches depending on 2α (from [31])

notches (i.e. weld toes and roots) to be included in the same diagram (whereas the N-SIFs have different units). A presentation of the results for 650 welded joints has been given by Lazzarin et al. [20], see Fig. 21 (mostly transverse non-load carrying fillet-welded joints)

A uniform control radius R_0=0.28 mm has been used for both weld toe and weld root failure. The thickness of the main plate ranged from 6 to 100 mm, so that its effect is included. The scatter band given in Fig. 21 refers to ±2 standard deviations, giving a characteristic fatigue strength of $\Delta\overline{W} = 0.058$ Nmm/mm^3.

A relationship with stresses can be found using the simple expression

$$\Delta\sigma_{eq} = \sqrt{2E' \times \Delta\overline{W}} \tag{3.17}$$

with $E'=E/(1-\nu^2)$ for plane strain conditions [20]. Equation (3.17) describes the equivalent stress for a calculated SED averaged over a definite volume. Using this equation, the vertical axis in Fig. 21 could be converted into an equivalent stress range, resulting in a slope exponent m=3 because of the square root in Eq. (3.17).

An alternative approach based on the N-SIF is the so-called *Peak Stress Approach* proposed by Meneghetti [27, 28]. This approach utilises the ratio K_{FE}* between the notch stress intensity factor K_1 and the nodal stress σ_{peak} in the V-shaped notch for a finite element mesh with given global element size d and displacement functions, which is valid as long as the mode II stress contribution to the local stress field is absent or negligible. In the case of a mesh where only two elements share the nodal point in the weld toe and four elements the one in the weld root (see Fig. 22), the following relationship has been found for certain linear 2D elements (PLANE42 of ANSYS element library):

$$K^*_{FE} = \frac{K_1}{\sigma_{peak} \times d^{1-\lambda_1}} \cong 1.38 \tag{3.18}$$

It should be borne in mind that this and the following relations are only valid for the element type mentioned. The opening angle α may be between 0 and 135°. It must be taken into account that different element types and mesh patterns lead to different peak stress values, mainly because of varying internal element stresses and stress extrapolation rules from the integration points to the nodal points.

A link between the range of the peak stress $\Delta\sigma_{peak}$ and the strain energy density SED averaged within the control radius R_0 was found by Meneghetti and Lazzarin [29] by using the range of the equivalent stress $\Delta\sigma_{eq}$, resulting in:

$$\Delta\sigma_{eq} = f_w \times \Delta\sigma_{peak} = 1.38 \times \sqrt{\frac{2e_1}{1-\nu^2}} \times \Delta\sigma_{peak} \times \left(\frac{d}{R_0}\right)^{1-\lambda_1} \tag{3.19}$$

The range of the average strain energy density is given by Eq. (3.16). The factor f_w is listed in Table 2 for the factor in Eq. (3.19), ν=0.3, d=1 mm, R_0=0.28 mm and λ_1 and e_1 according to Lazzarin and Zambardi [19].

The weighted peak stress range $f_w \times \Delta\sigma_{peak}$ can be used as an alternative parameter for an S–N curve [29].

In general it can be said that the approaches based on the notch stress intensity factor offer similar opportunities and benefits to those of the effective notch stress approach. One advantage is that the original idealised weld geometry can be

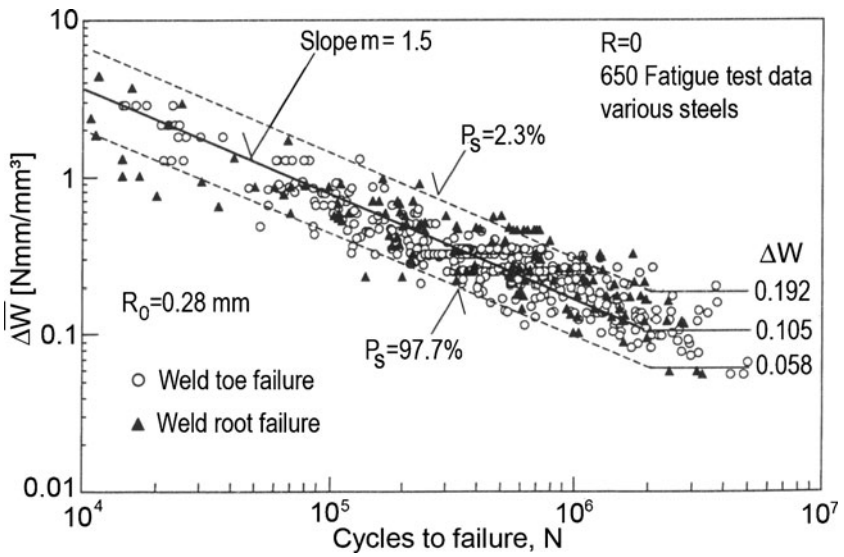

Fig. 21 Fatigue strength of fillet-welded joints as function of the range of the average strain energy density $\Delta\overline{W}$ [20]

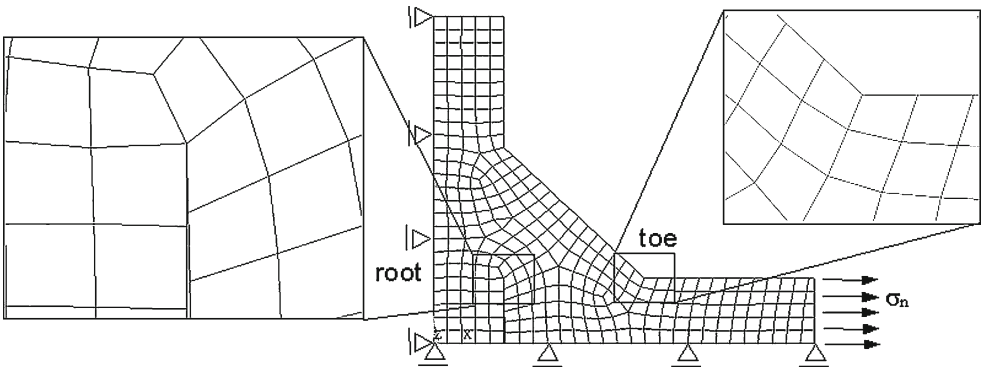

Fig. 22 Pattern of finite elements to analyse a welded joint by means of the Peak Stress Method [29]

used without inserting the fictitious notch radius, which might affect geometry, particularly at weld roots. The validation includes weld roots in addition to weld toes. The other limitations are the same as for all approaches based on S–N curves.

3.5.2 Computation of notch stress intensity factors or strain energy density

Different possibilities exist for computing the stress parameter for the application of the notch stress intensity factor approach described above:

- Direct computation of the notch stress intensity factor N-SIF. As mentioned before, this requires an extremely fine finite element mesh [41] from which the stress distribution can be compared with the theoretical solution of V-notches to derive the N-SIFs.
- Computation of the average SED in a control volume with radius R_0 allowing the N-SIF to be derived (Eq. 3.16). Alternatively, the SED or the equivalent stress can be used directly for the fatigue assessment. The approach requires finite element sizes of R_0 or less.
- Lazzarin et al. [20] have shown that the computation of the average SED for a larger control radius of R^*=1 mm and converting it to 0.28 mm using Eq. (3.16) yields results with sufficient accuracy at the weld toe where only mode I stress distribution is singular. In principle, Eq. (3.16) can also be used under mixed mode conditions when the degree of singularity of the mode I and mode II stress fields is the same, as at the weld root region ($\lambda_1=\lambda_2=0.5$).
- However, at the roots of non-penetrating welds with loading parallel to the slit, the effect of the T-stress (i.e. the constant stress component parallel to the slit [47]) has to be taken into account. This means that the main contribution of the T-stress σ_T to the strain energy density at weld roots, i.e.

$$\Delta\overline{W}_T = \sigma_T^2 \Big/ 2E', \tag{3.20}$$

has to be deducted from the average strain energy $\Delta\overline{W}$ (R^*) before converting the strain energy density by Eq. (3.16). By so doing, it is possible to compute the increase to the local strain energy density due only to the singular stress fields. After conversion ΔW_T must be included again. The calculation remains approximate because the effect of further terms [21] has not been considered here for the sake of simplicity.
- Computation of the peak stress σ_{peak} and converting it into the notch stress intensity factor (Eq. 3.18) or the SED (Eq. 3.19 and 3.17). A typical FE mesh has been shown in Fig. 22.
- Figure 23 shows a fine-meshed FE model for the 2D analysis of the average SED in a control volume with R_0=0.28 mm at the weld toe as well as the weld root. The alternative with a coarse mesh is illustrated in Fig. 24, using triangular elements around the notch tip having quadratic shape function

Table 2 Parameters for Eq. (3.19) for ν=0.3, d=1 mm and R_0=0.28 mm [29]

2α (deg)	λ_1	e_1	f_w
0	0.500	0.133	1.410
90	0.544	0.145	1.392
110	0.586	0.136	1.278
120	0.616	0.129	1.198
125	0.633	0.126	1.159
135	0.674	0.118	1.064
145	0.723	0.109	0.961
150	0.752	0.104	0.905

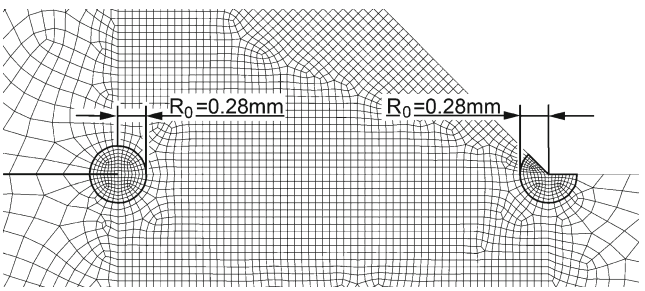

Fig. 23 FE model for the computation of the SED at a weld toe (*right*) and weld root (*left*)

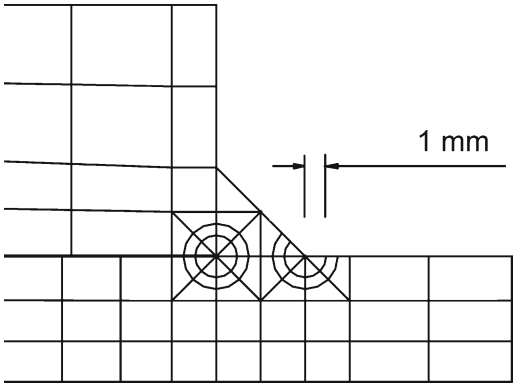

Fig. 24 Coarse mesh for the SED computation

and a length of 1 mm. Suggestions for meshing and several applications have been shown by Lazzarin et al. [20] and Fischer et al. [9].

3.6 Crack propagation approach

3.6.1 Overview of the approach

The crack propagation approach allows the phase of crack growth between an initial and a final crack length to be evaluated. This is based on *linear elastic fracture mechanics*, as plastic zones are rather small during fatigue crack propagation. The crack propagation rate da/dN can be estimated using the stress intensity factor at the crack tip and the power law by *Paris and Erdogan*, describing the linear relationship between the crack propagation rate and the range of the stress intensity factor ΔK in bi-logarithmic scale:

$$\frac{da}{dN} = C \times \Delta K^{\mathrm{m}} \tag{3.21}$$

with the material parameters C and m. The linear relationship is valid between the threshold value ΔK_{th} with no crack propagation beneath and the transition to an unstable fracture with the critical stress intensity factor K_{c}, see Fig. 25. Different variants exist to consider, e.g. the stress ratio R.

The approach is well suited to the fatigue assessment of welded joints where the crack initiation life is short and the fatigue life is mainly determined by the crack propagation phase. This is particularly the case for weld root fatigue where the slit between the non-fused root faces acts like an initial crack. In contrast to the S–N approaches, which are based on one stress value, the effect of the complete stress field on fatigue is considered. This increases the analysis effort but offers a better fatigue life estimation in several cases.

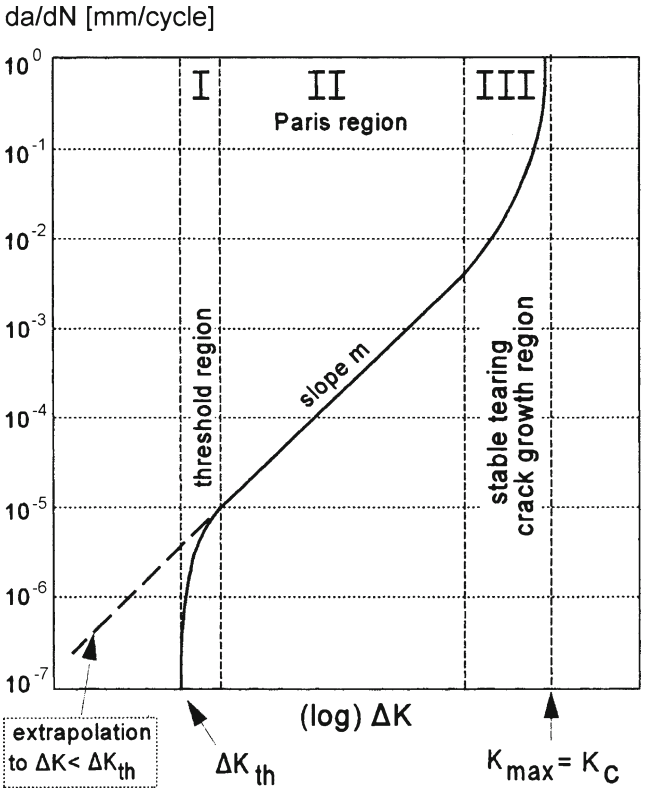

Fig. 25 Example for relationship between the crack growth rate da/dN and the range of the stress intensity factor ΔK [31]

In the following, some remarks are given on the application of the approach to weld root fatigue. Further information on the approach can be found in the relevant literature (e.g. [2, 7, 16, 31, 33]).

3.6.2 Stress intensity factors

As a first step, stress intensity factors have to be determined for different crack lengths or shapes. Different possibilities exist, such as the use of tabulated factors in handbooks and the application of numerical methods. Here, the stress intensity factors can be determined indirectly by the so-called weight factor method or directly by the finite element method, using the strain energy release rate during virtual or real crack extension or the J-integral.

Finite element models have to be very fine-meshed around the crack tip. If isoparametric elements with mid-side nodes are used, the results can be improved by using a special feature, i.e. shifting the mid-side nodes nearer the crack tip to the quarter points in all elements around the crack tip (preferably elements of triangular shape), see Fig. 26. In this case, they fulfil the $r^{-0.5}$ singularity of the local stress field.

It is important to consider the local geometry around the crack and the loading, which is taken into account by the so-called *geometry factor* in standard cases. Also, the crack shape and crack path may affect the results considerably.

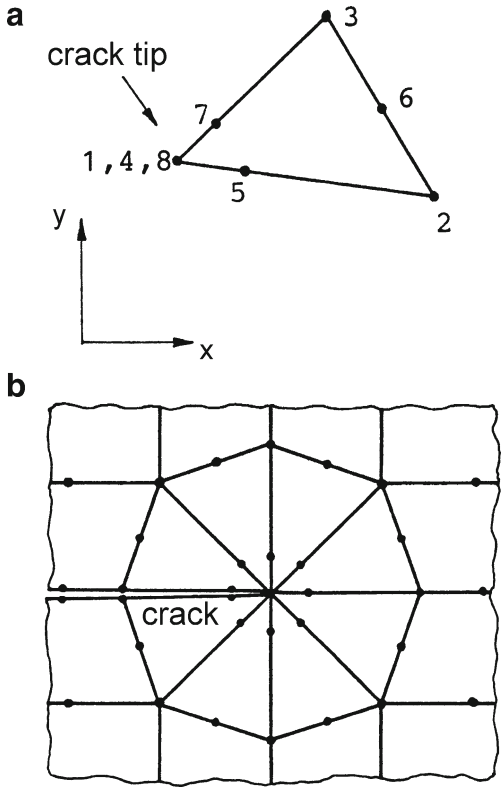

Fig. 26 Isoparametric element **a** with shifted mid-side nodes (quarter point) and **b** modelling

The crack may be assumed as a continuous 2D crack or a local crack with semi-elliptical shape. If a long non-fused slit acts as an initial crack, a continuous 2D crack is usually assumed. The crack path is mainly determined by the ratio between the stress intensity factors for the sliding mode K_{II} and opening mode K_I. A pronounced K_{II} (shear mode) results in a deviation of the crack path in a direction which is perpendicular to the max. principal stress (range).

3.6.3 Determination of fatigue life

The fatigue life consumed by crack propagation is determined by integrating the power law (3.21) of Paris and Erdogan. Material constants C and m as well as ΔK_{th} are proposed in different guidelines (e.g. [6, 16]), assuming upper bound values for predictions on the safe side.

The critical crack length or stress intensity factor K_c affects the crack propagation only marginally, as the crack growth rate is already very high when the linear relationship (Eq. 3.21) approaches K_c.

Crack closure may be more important, making the stress cycle effective only during the portion where the crack is open. This can be smaller than the tensile part of the stress cycle because of local plastification. Usually, an effective part of the range of the stress intensity factor ΔK_{eff} is defined for the determination of the crack growth rate according to Eq. (3.21).

4 Demonstration examples

In total, six demonstration examples are described. Table 3 gives an overview of the different approaches applied. For each approach, at least two examples are given.

4.1 Cruciform joint

4.1.1 Description of the detail

The cruciform joint with partial penetration shown in Fig. 27 is selected as example. The chosen geometry parameters are:

Plate thickness	$2b$=25.0 mm
Length of root face	$2a$=12.5 mm
Leg length	c=17.7 mm (=12.5·√2 mm)

In Fig. 27, this geometry is just below the limit curve for 25 mm so that the fatigue strength computed for the weld toe should be slightly above that for the weld root. The characteristic fatigue strength based on nominal axial stress range is to be determined for weld toe and weld root failure.

4.1.2 Application of the nominal stress approach

In the nominal stress approach, *weld toe failure* in partial penetration cruciform joints is frequently associated with

Table 3 Demonstration examples and approaches applied

Example	Nominal stress approach	Structural stress approach	Eff. notch stress approach	Approach based on N-SIF	Crack propagation approach
Cruciform joint	X	X	X	X	X
Fillet weld around attachment end		X		X	
One-sided fillet weld around RHS joint	X	X	X		
Lap joints and cover plates	X		X	X	X
Fillet-welded pipe penetration	X		X		
Laser-stake welded T-joint	X		X	X	X

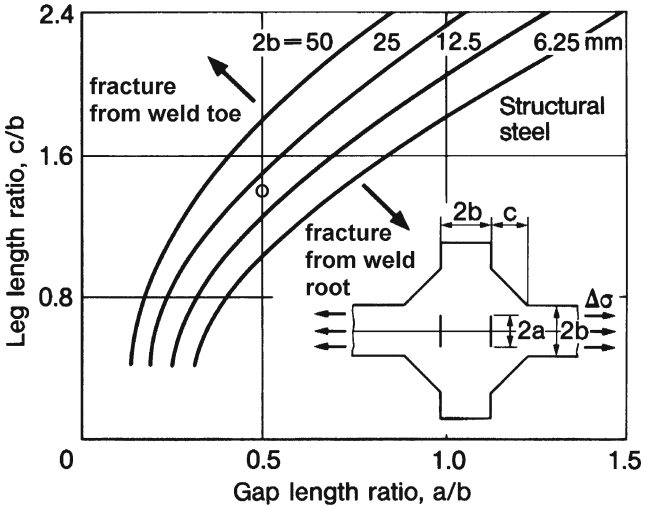

Fig. 27 Limit curves separating weld toe and root fracture in cruciform joints [24], the geometry investigated here is indicated by a *circle*

fatigue class FAT 63, see No. 413 in the IIW Fatigue Design Recommendations [16]. *Weld root failure*, however, is associated with FAT 36, based on nominal weld stress. If the throat thickness is defined by the shortest distance between the end of the slit and the weld surface, i.e. 16.9 mm in the example, the ratio between the stresses in the weld throat and in the plate is 0.739, so that the fatigue class for weld root fatigue becomes FAT 49 if based on plate stress. This means that weld root fatigue is more critical than weld toe fatigue which agrees well with Fig. 27.

4.1.3 Application of the structural stress approach

The 2D finite element model shown in Fig. 28 was created assuming plane strain condition. The axial load is applied at the right end (σ_n=100 MPa).

For fatigue assessment of the *weld toe*, stress values were extracted at a distance 0.4*t* and 1.0*t* on the plate surface and linearly extrapolated to the weld toe [16], yielding a structural hot-spot stress of σ_{hs}=100.8 MPa.

For fatigue assessment of the *weld root*, nodal forces were extracted in the vertical weld leg section and summed up according to Fig. 13 and Eqs. (3.12–3.13). This gives the following results:

- membrane stress in weld leg $\sigma_{m,w}$=52 N/mm^2
- bending stress in weld leg $\sigma_{b,w}$=67 N/mm^2
- structural stress in weld leg $\sigma_{s,w}$=119 N/mm^2

The transverse shear stress in the weld is within the limits of the approach (τ_w=14 N/mm^2), i.e. less than 20 % of the structural stress.

The structural stresses at the weld toe, σ_{hs}=100.8 MPa, and at the weld root, $\sigma_{s,w}$=119 MPa, are compared with their corresponding fatigue classes (FAT90 at toe and FAT80 at root). The ratios between structural stress and the corresponding fatigue class show an advantage for root failure. Based on nominal stress in the main plate, the characteristic fatigue strengths are 89 MPa for the weld toe and 68 MPa for the weld root.

The alternative with shell elements described in Section 3.3.3 shows smaller bending stresses in the weld; hence, it is on the non-conservative side.

4.1.4 Application of the effective notch stress approach

The 2D finite element model shown in Fig. 29 has been created representing one quarter of the joint. Symmetry conditions have been utilised at the left und lower boundaries. 2D plane strain elements with quadratic shape function have been used. The mesh fineness in the critical points, i.e. in the weld toe and weld root (modelled by a keyhole notch), corresponds to the recommendations by Fricke [12]. An axial load is acting on the right-hand side.

The following fatigue notch factors K_f at the weld toe and root, based on the stress in the abutting plate, have been computed:

- Weld toe, K_f=3.75
- Weld root, K_f=4.43

The notch stress at the weld root is about 18 % higher than that at the weld toe which agrees with Fig. 27 where weld root fatigue is more critical.

4.1.5 Application of the strain energy density approach

The calculation of the strain energy density (SED) $\overline{W}$ averaged within a control radius of R_0=0.28 mm with

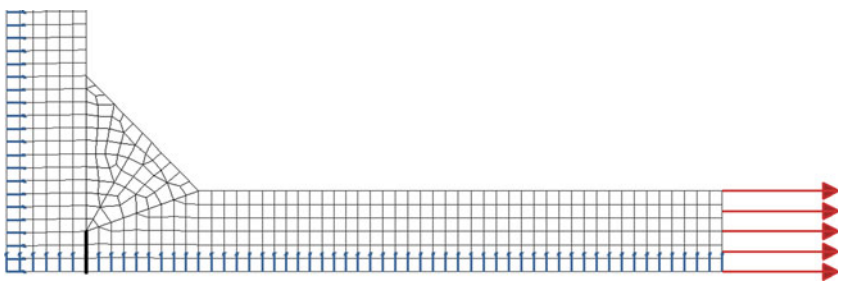

Fig. 28 Finite element model (1/4 model), boundary conditions and loading

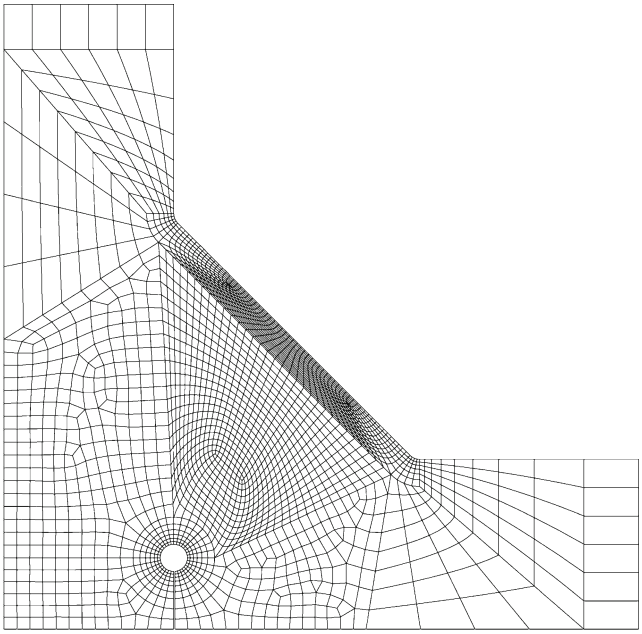

Fig. 29 Finite element model (1/4 model) for numerical analysis of the effective notch stress

the finite element model shown in Fig. 30 yields the following values at the weld toe and root for an axial stress of 100 N/mm^2.

- Weld toe, $\overline{W} = 0.192\ Nmm/mm^3$
- Weld root, $\overline{W} = 0.224\ Nmm/mm^3$

Here, the SED at the weld root is about 17 % higher than that at the weld toe.

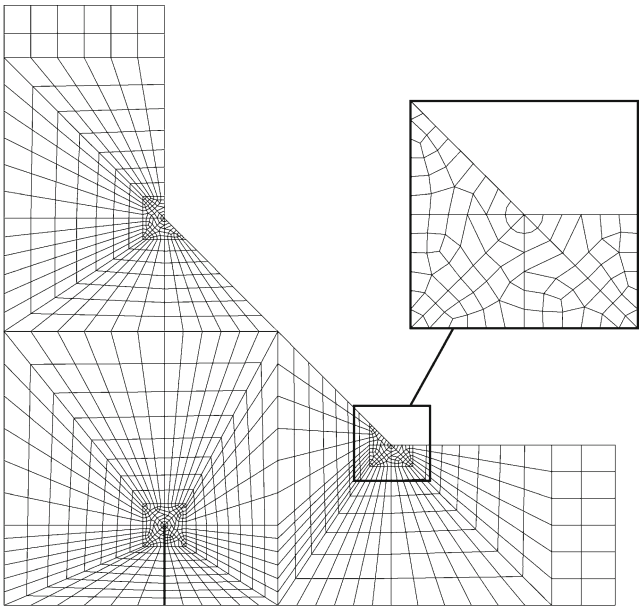

Fig. 30 Finite element model (1/4 model) for numerical analysis of the average strain energy density

4.1.6 Application of the Peak Stress approach

According to Meneghetti and Lazzarin [29], the weighted peak stress is determined at the toe and root of the joint. A free mesh of four-node quadrilateral elements (PLANE 42 elements of the ANSYS element library) shown in Fig. 31 was adopted in the numerical analysis, and the global element size was set to 1 mm. The maximum principal stress at the toe and root locations was determined and then multiplied by the coefficient f_w reported in Table 2. The resulting equivalent stresses obtained for an axial stress of 100 N/mm^2 are included in Fig. 31, showing that root failure rather than toe failure is predicted, with the stress being 18 % higher.

4.1.7 Application of the crack propagation approach

The crack propagation approach is applied using the Paris–Erdogan law (Eq. 3.21) with material parameters m=3 and C=5.21·10^{-13} (units, Newton and millimeters) recommended by Hobbacher [16], representing the upper limit of the scatter band (2.3 % probability of failure). The fatigue life is computed for a constant stress range $\Delta\sigma_n$=100 N/mm^2. End of life is defined when the crack length reaches half the plate thickness for toe cracks and half the throat thickness for root cracks. The remaining lifetime is rather short.

Crack propagation from the weld root The length of the weld root face (12.5 mm) is assumed as the initial crack length. A continuous 2D crack is assumed for the whole propagation phase so that a 2D model is sufficient for the numerical analysis of the stress intensity factor (SIF). The finite element method was applied using the program FRANC2D [49]. Figure 32 shows the basic mesh created with 2D elements having quadratic displacement function. Plane strain was assumed. Symmetry conditions were utilised in two planes resulting in a quarter model.

Figure 32a also shows the computed crack path, which is slightly curved due to the presence of K_{II}. The fatigue life up to a crack length of half the weld throat thickness is 265,000 cycles.

Crack propagation from the weld toe Two numerical analyses were performed. The first again assumes a continuous 2D crack. Figure 32b shows the basic mesh created for the computation in FRANC2D [49], again indicating a curved crack front.

The initial crack length was assumed as a_i=0.15 mm, as recommended by Hobbacher [16]. The resulting fatigue life up to a crack length of half plate thickness was found to be 143,000 cycles. This is much shorter than the crack propagation life of the weld root, which does not correspond to Fig. 27. Even a much smaller initial crack length of a_i=0.05 mm does not change this, as the fatigue life would increase only to 158,000 cycles.

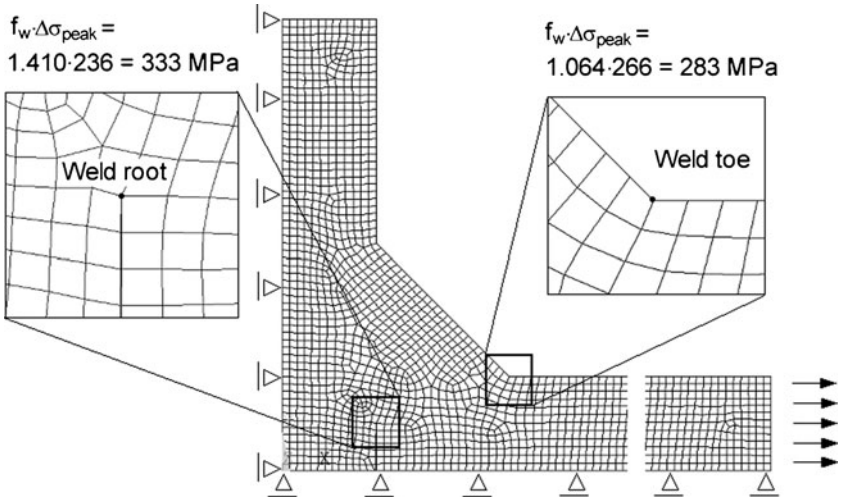

Fig. 31 The Peak Stress Method applied to estimate toe or root failure of a cruciform joint

A possible explanation for the unexpected result is the assumption of a continuous 2D crack at the weld toe, whereas semi-elliptical cracks initiating from small defects or high notch effects are often observed in practice. Therefore, a second analysis of the SIFs with a 3D model was performed, using the program ANSYS 13.0 offering an iterative approach for the development of the crack front.

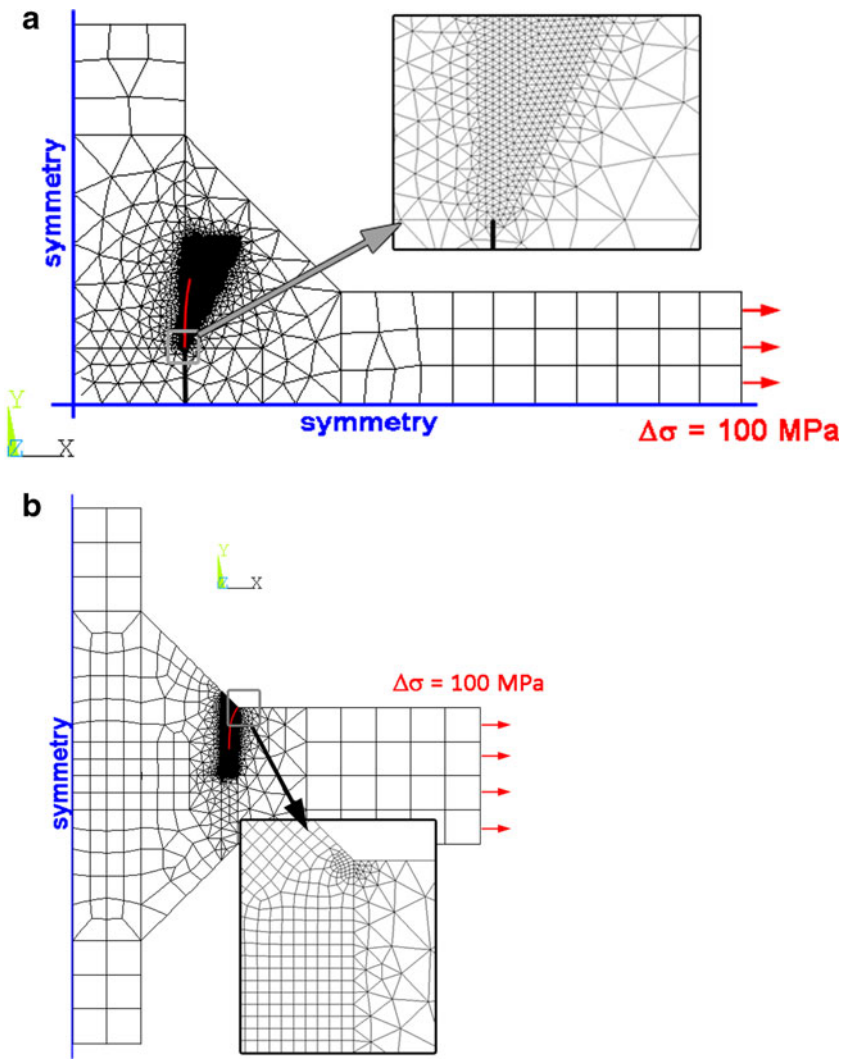

Fig. 32 Finite element models for numerical analysis of stress intensity factors **a** at the weld root and **b** at the weld toe

Figure 33 shows the finite element model chosen. The width of the model was assumed to be 50 mm, being typical for fatigue test specimens. The model consists of solid elements with quadratic displacement function. Along the semi-elliptical crack front, elements with mid-side nodes shifted towards the crack front, i.e. to the quarter points, were used to model the stress singularity, see Fig. 26. Symmetry conditions were utilised at half width.

The SIFs of the semi-elliptical shape were again computed at the vertex points. In order to avoid any influence of the singularity of the sharp weld toe at the outer vertex point (see right part of Fig. 33), the stress intensity factor at this point has been calculated by quadratic extrapolation of the adjacent results along the crack front.

The initial crack has been assumed to be semi-circular with $a_i=c_i=0.15$ mm. The development of the crack front was assumed in accordance with the computed stress intensity factors at the vertex points, using the iterative approach mentioned. The iteration ended with a crack depth of 3.6 mm at 292,000 load cycles. Afterwards, a 2D crack is assumed, resulting for instance from coalescence of neighbouring cracks. This 2D crack reaches half plate thickness after a total of 324,000 load cycles.

The crack propagation life calculated in the 3D analysis with semi-elliptical crack shapes is much longer than that computed with 2D cracks. Furthermore, it is also longer than the computed life for the weld root crack (265,000 cycles) which is in agreement with Fig. 27.

4.1.8 Comparison of the results

A comparison between all results can be performed on the basis of the characteristic fatigue strength $\Delta\sigma_c$ at $2{\cdot}10^6$ cycles for survival probability P_s=97.7 % referring to *nominal plate stress* which can be derived from the computed local stress or SED, the assumed nominal stress and the characteristic value of the S-N curve. The latter has been assumed as FAT 225 for the effective notch stress and 0.058 Nmm/mm^3 for the characteristic SED, see Fig. 21.

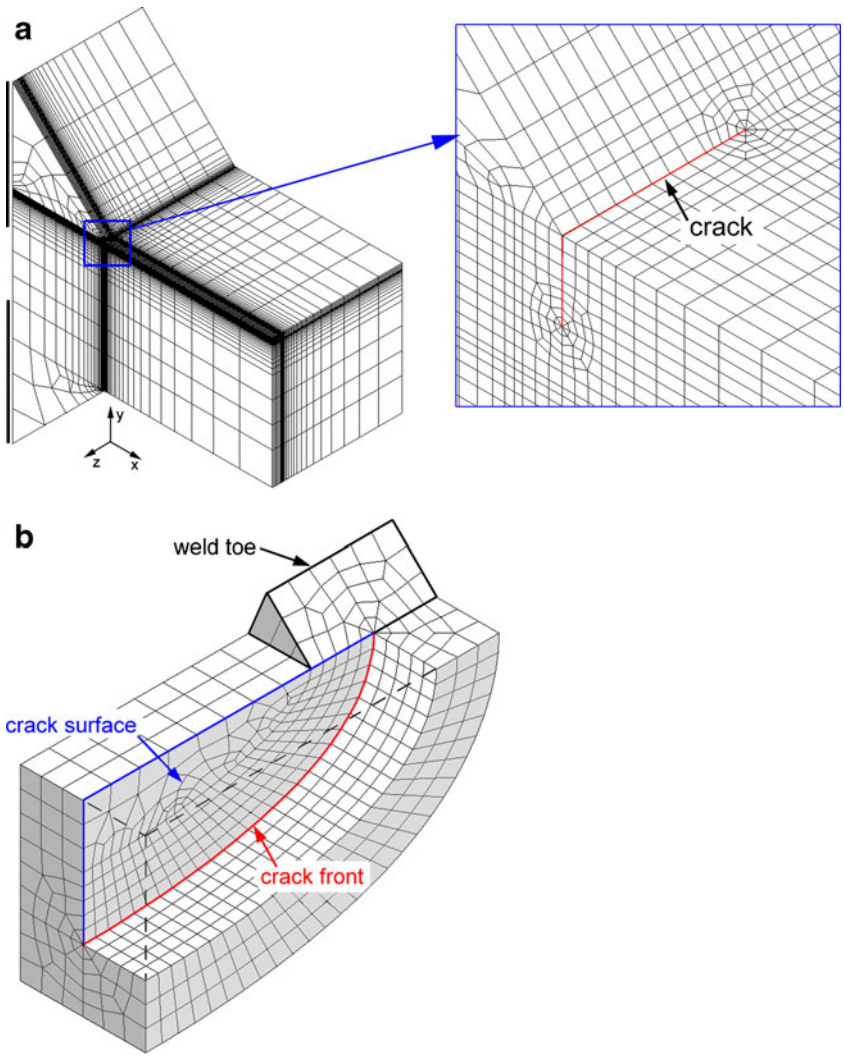

Fig. 33 Finite element model (half model) for numerical analysis of stress intensity factors at the weld toe (3D model) and details of crack modelling

Regarding the Peak Stress Method, the SED can be derived from the equivalent stress using Eq. (3.17). All approaches show that weld root failure is more probable, which is in agreement with Fig. 27, see Table 4. There are some differences between the results which include the test results evaluated by Maddox [24].

The results of the approaches, except for the nominal stress approach, do not yet consider the effects of axial misalignment. If a misalignment of 15 % of the plate thickness is assumed, the secondary bending stress is particularly high at the *weld toe*, resulting in a stress magnification of k_m=1.45 according to Eq. (3.1). For the *weld root*, the corresponding Eq. (3.2) yields k_m=1.09. This would mean that the results of the structural and nominal stress approaches are closer together. The notch stress, strain energy and crack propagation approaches are more conservative than the aforementioned ones and would then expect crack initiation at the weld toe. Their assessment might be valid, as it remains unclear to what extent axial misalignment was present in the tests forming the basis of Fig. 27.

4.2 Fillet weld around attachment end

4.2.1 Description of the detail

Figure 34 shows a specimen designed for the investigation of weld toe and root failure at attachment ends. The load in the plate is transferred into the attachments by shear stresses parallel to the weld which has a throat thickness a=4 mm. In addition, pronounced bending stresses are acting in the attachments. The fatigue-critical detail is the soft nose of the right-hand attachment in Fig. 34, where the fillet weld is subjected to axial and shear stresses.

As the detail is relatively complex, only the structural stress and the stress intensity approaches are applied, allowing the fatigue strength of the weld toe and the weld root at the end of the attachment to be assessed.

Table 4 Characteristic fatigue strength $\Delta\sigma_c$ based on nominal stresses in the main plate

	$\Delta\sigma_c$ (N/mm^2)	
	At weld toe	At weld root
Nominal stress approach	63	**49**
Structural stress approach	89	**68**
Effective notch stress approach	60	**51**
Strain energy approach	55	**51**
Crack propagation approach	55	**51**
Fatigue test results based on Maddox [24]	68	**63**

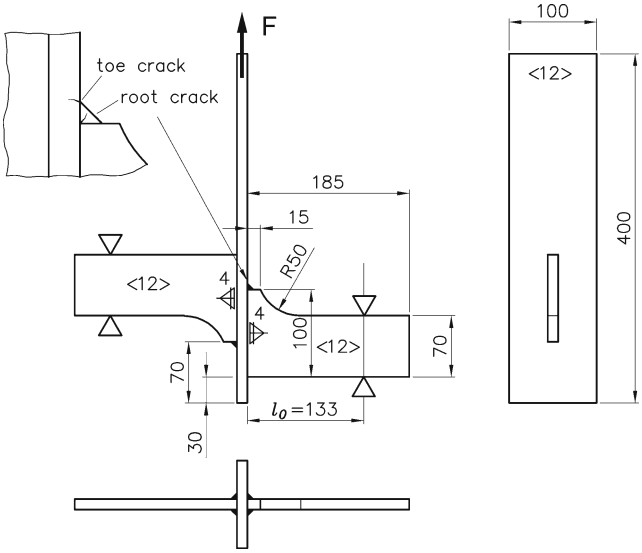

Fig. 34 Specimen with attachments on a plate

4.2.2 Fatigue tests

Constant amplitude fatigue tests were performed with a total of

- twenty specimens in as-welded state with a nominal stress range $\Delta\sigma_n$=28 N/mm^2 and 20 N/mm^2 at a stress ratio R≈0
- ten specimens in as-welded state with $\Delta\sigma_n$=23.5 N/mm^2 at R=0.5
- ten specimens in stress-relieved state with $\Delta\sigma_n$=20 N/mm^2 at R≈0

The tests, which are described by Fricke and Doerk [13], showed weld root failure in almost all specimens. The detailed results will be used in the subsequent investigations for comparison with the approaches.

4.2.3 Application of the structural stress approach with solid elements

The stresses were computed for a force in the vertical plate of F=50 kN, corresponding to a nominal stress of σ_n=41.7 N/mm^2. A relatively coarse finite element model was created which is shown in Fig. 35 together with the deformations and distribution of the max. principal stress.

The structural hot-spot stress at the upper weld toe, calculated acc. to [16], amounts to σ_{hs}=267 N/mm^2, which means a structural stress concentration factor K_s=6.4 referring to the nominal stress in the vertical plate strip.

The bending moment in the transverse attachment creates a *nominal* bending stress in the weld throat of $\sigma_{n,w}$=183 N/mm^2, based on the section modulus of the weld throat area concentrated at the root line. More relevant is the *local nominal* stress at the end of the weld, which has been derived with the approach illustrated in Fig. 12b. An

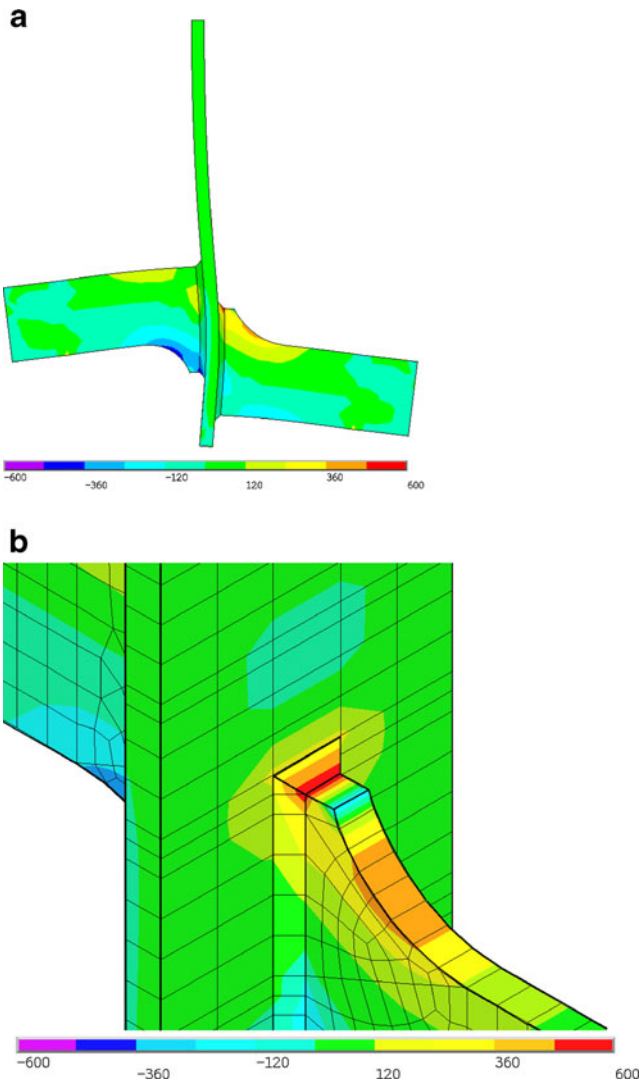

Fig. 35 Finite element model of the specimen with deformations and max. principal stress distribution

inclination angle of φ=32.6° was found for the principal stress in the reference area (t×t/2). The local nominal stress in the effective weld area according to Eq. (3.9) results in $\sigma_{n,w,loc}$=346 N/mm^2, which is almost twice as high as the nominal stress in the weld. The evaluation of the weld stresses according to Eq. (3.8) and Fig. 12a gave almost the same result (337 N/mm^2).

The fatigue assessment in Table 5 is performed by comparing the local stress ranges for a cyclic force of ΔF=50 kN

Table 5 Local stress ranges for ΔF=50 kN and characteristic fatigue strength (FAT)

Crack initiation site	Nominal stress range $\Delta\sigma_n$ (N/mm^2)	Computed local stress range (N/mm^2)	FAT class (local approach)
Weld toe	41.7	$\Delta\sigma_{hs}$=267	90
Weld root	41.7	$\Delta\sigma_{n,w,loc}$=346	40

and the corresponding FAT classes. FAT 90 is assumed here for partial-load carrying weld toes on a plate surface. The comparison of the numbers shows that root cracking is much more probable than toe cracking due to the smaller ratio between endurable stress (FAT class) and applied stress range.

The fatigue lives from the tests are plotted in Fig. 36 in relation to the range of the local nominal weld stress $\Delta\sigma_{n,w,loc}$. They show that the results are only slightly affected by the stress ratio R and the residual stresses, which is in contrast to relatively stiff attachment ends where compressive residual stresses have been observed in the attachment.

The figure also shows that FAT 40 is a good basis for fatigue assessment, as the characteristic fatigue strength of the test series is slightly above this class. This was also shown for other tested geometries with different toe radii and weld throat thicknesses [13].

4.2.4 Application of the structural stress approach with shell elements

For the same load condition (F=50 kN), the finite element analysis has been performed using shell elements and the technique described in Fig. 14. Mesh nodes have been introduced at the t/2 reference locations according to Fig. 11. The von Mises stress distribution is displayed in Fig. 37a. Structural hot-spot stress is calculated using through-thickness forces integration over the weld boundary as shown in Fig. 37b. The structural hot-spot stress range in the plate at the attachment end was found to be $\Delta\sigma_{hs}$=254 N/mm^2 (5 % less than in the solid model).

The local nominal weld stress is calculated with the forces extracted from the attachment (see Fig. 38) and Eq. (3.9) with φ=36.4°, resulting in $\sigma_{n,w,loc}$=368 N/mm^2 (6 % more than the solid model).

Related to their respective fatigue classes of FAT90 for the weld toe and FAT40 for the weld root, the highest ratio is

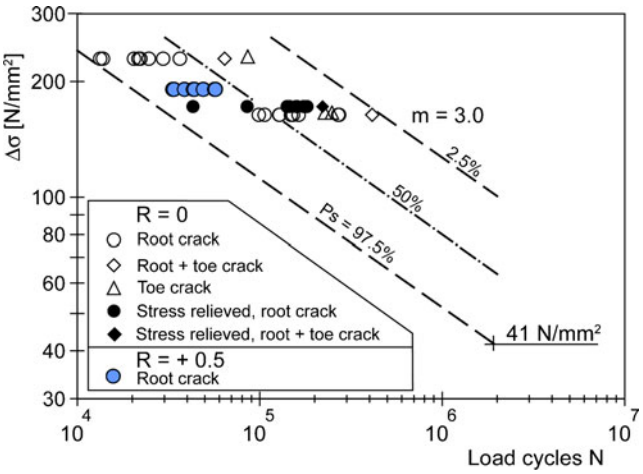

Fig. 36 S-N results from tests (Δσ=local nominal stress in weld)

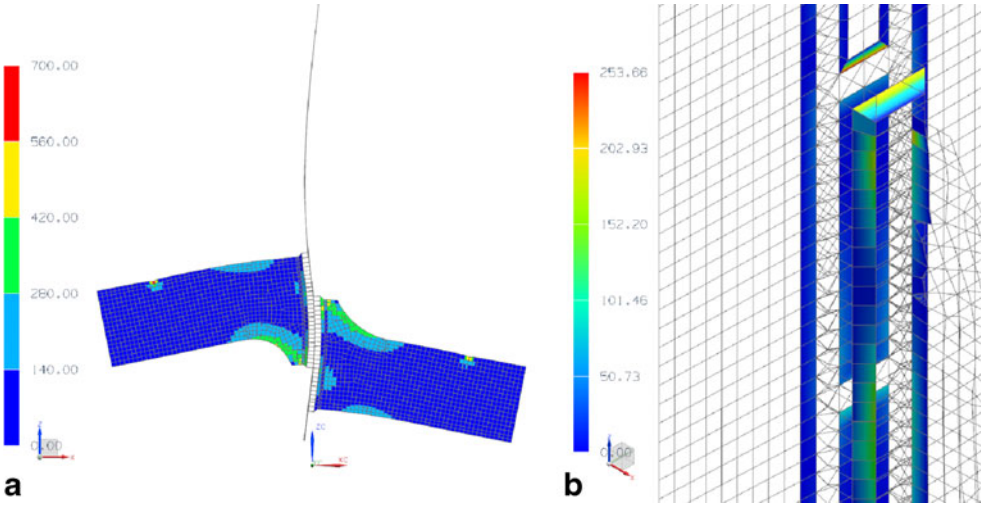

Fig. 37 Shell element model of the specimen with deformations and von Mises stress distribution (**a**) and structural stress range over the weld contour (**b**) in MPa

obtained at the weld root where the crack might occur. The stresses calculated with shell elements are slightly larger than those from the solid model described above.

4.2.5 Application of the strain energy density approach

The strain energy density approach based on the notch stress intensity factor has been applied to this detail by Lazzarin et al. [21]. A nominal stress of σ_n=100 N/mm^2 was assumed in the vertical plate strip. The strain energy density has been evaluated by means of 3D finite element analysis using 20 node brick elements. A 3D circular sector with R^*=1 mm surrounding the crack initiation points has been used and then reconverted to R_0=0.28 mm by means of the following equation, based on Eq. (3.16) neglecting K_2.

$$\frac{\overline{W}(0.28mm)}{\overline{W}(1.0mm)} = \left(\frac{0.28}{1.0}\right)^{2(\lambda_1-1)} \tag{5.1}$$

Table 6 shows the computed strain energy densities for the weld toe and weld root. It turns out that the weld root is more critical (for R_0=0.28 mm). Figure 39 shows the test data in an S-N diagram based on the range of the strain energy density $\Delta\overline{W}$. The results agree well with the scatter band proposed by Lazzarin et al. [20], see also Fig. 21.

4.3 One-sided fillet weld around rectangular hollow section joint

4.3.1 Description of the detail

The third detail is a fillet-welded connection between two rectangular hollow sections (RHS), see Fig. 40. The dimensions of the RHS are 120×80×6 mm (height×width×thickness). Two hollow sections are connected to a 15-mm-thick intermediate plate by a single-sided fillet weld. Two types of welding process were applied: manual metal-arc welding with covered electrode, resulting in a mean throat thickness of a=4.3 mm, and the MAG process with flux-cored wires, resulting in a=5.1 mm. The gap between the intermediate plate and the hollow section is assumed to be zero, see "DET A" in Fig. 40.

Two load cases were investigated:

1. axial load at the end of the RHS, applied to nine of the manual metal-arc welded specimens

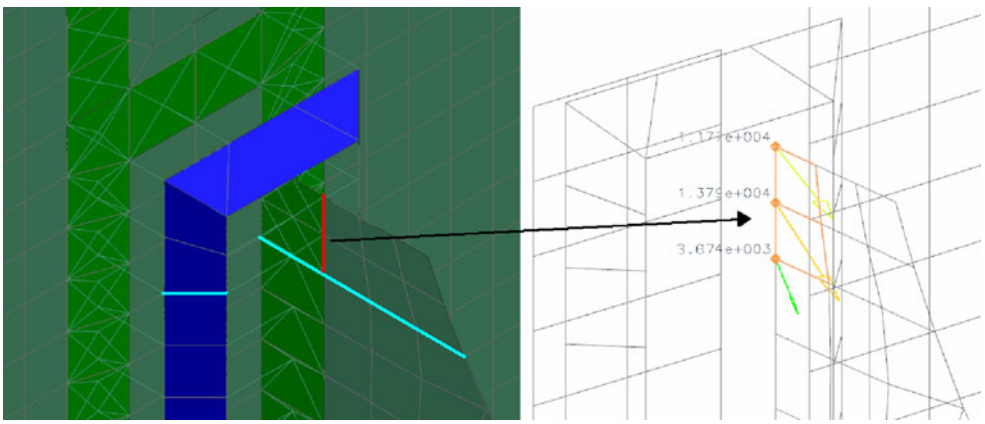

Fig. 38 Nodal forces extracted from the shell model

Table 6 Mean values for the average strain energy density $\Delta\overline{W}$

Crack initiation site	Nominal stress range $\Delta\sigma_n$ (N/mm^2)	$\Delta\overline{W}$ for R^*=1 mm (Nmm/mm^3)	$\Delta\overline{W}$ for R_0=0.28 mm (Nmm/mm^3)
Weld toe	100	6.546	15.010
Weld root	100	5.329	19.030

2. vertical three-point bending, applied to six of the manual metal-arc welded specimens and seven MAG-welded specimens

In the stress analysis, symmetry conditions were utilized, and a constant stress of 100 N/mm^2 was applied to the right end. In the bending load case, a distributed shear force of 17.25 N was applied to the right end creating the nominal bending stress of 100 N/mm^2 at the weld.

4.3.2 Fatigue tests

The fatigue tests were performed with constant load amplitudes and a frequency of approximately 30 Hz. A high stress ratio R=0.5 was chosen according to the IIW Fatigue Design Recommendations [16]. One or two load levels were selected for the tests of each series of specimens. All specimens failed due to root cracking. The failure criterion for terminating the tests was a through-thickness crack. After this, the remaining life of the specimens was very short.

The test results, which are further described by Fricke et al. [15], are shown in Fig. 41 in terms of the nominal stress range in the RHS member at the weld. The S-N curves given for a probability of survival of 50 and 97.7 % were obtained from statistical analysis assuming a fixed slope exponent m=3. The results for the bending load show that the welding process affects fatigue life, which is probably due to differences in the sharpness of the weld root.

4.3.3 Application of the nominal stress approach

In the IIW Fatigue Design Recommendations [16], this detail is classified as FAT 45 (structural detail no. 424). It should be borne in mind that the nominal stress for root failure is referred to the weld throat area.

When converting the nominal stress in the 6-mm-thick RHS wall to the weld throat thickness of a=4.3 mm and 5.1 mm, the tests under axial load show a fatigue class just below FAT 36, whereas the bending tests yield a fatigue class above FAT 45. The difference can be explained by the effect of local weld throat bending. Under axial load, the fatigue cracks appear at the long side of the RHS joint, which is less restrained with respect to local bending, whereas during bending they appear at the short upper side of the joint, which is the most highly stressed one and where local bending is more restrained.

The same reason might be responsible for the non-conservative fatigue assessment under axial load. Local approaches should be able to consider these effects.

4.3.4 Application of the structural stress approach using solid elements

The numerical analysis of the structural stress was performed with the finite element model shown in Fig. 42, using 20-node solid elements. Only one element was arranged over the wall and weld thickness. The axial loading is realised by the forces F1, while the force F2 creates the three-point bending.

The structural weld stress was analysed in the weld leg section according to Fig. 13 using the nodal forces. The last column of Table 7 shows the computed stress concentration factors $K_{s,w}$, i.e. the ratio between structural weld stress and nominal stress in the RHS member. The stress concentration factors clearly show the effect of increased local bending under axial load mentioned above. Furthermore, it can be

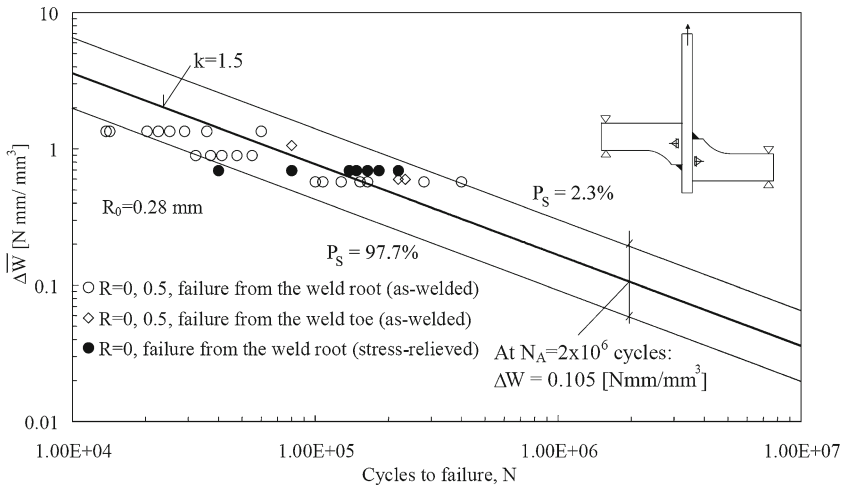

Fig. 39 S-N results in terms of the range of the average strain energy density $\Delta\overline{W}$ [21]

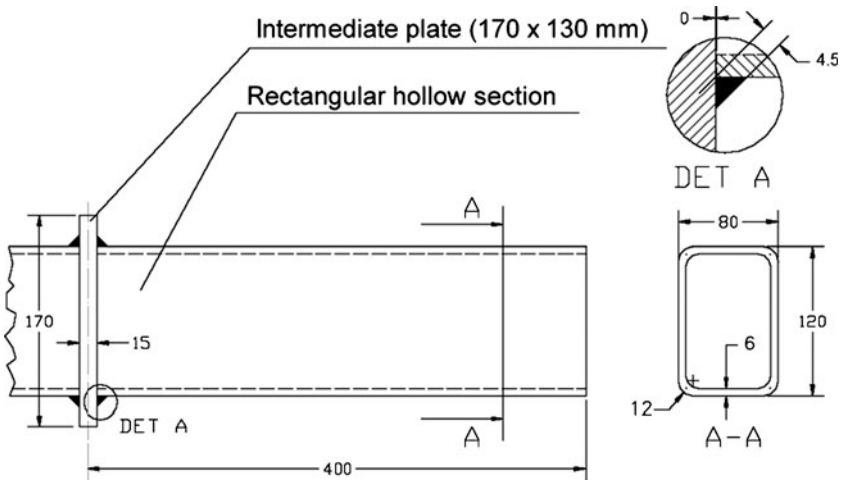

Fig. 40 Sketch of the fillet-welded end connection of an RHS member

seen that the weld throat thickness also influences the stress concentration factor, which explains the longer fatigue lives of the MAG-welded specimens as plotted in Fig. 41.

Figure 43 shows the test results in an S-N diagram lying well above the design S-N curve FAT 80 based on structural stress ranges mentioned earlier. It can be seen from Fig. 43 that the results for axial load are in the lower part of the scatter band, while those for bending load are in the upper part. This might be due to the more localised stress concentration under bending, resulting in semi-elliptical cracks showing slower crack propagation.

4.3.5 Application of the structural stress approach using shell elements

Corresponding finite element modelling is performed using shell elements and the technique described in Fig. 14. The structural stress is computed at the weld leg section according to Eqs. (3.11), (3.14), and (3.15). Figure 44 gives the distribution of the structural stress concentration factor along the weld line. For the axial load, maximum $K_{s,w}$ is obtained at mid-height of the RHS member, while for the bending load, it is located at mid-distance of the upper weld seam, which corresponds to the crack locations in the tests.

The maximum stress concentration factors $K_{s,w}$ are given in Table 8. These are about 10 % smaller than those calculated with the solid model (see Table 7). However, with these factors too the test results would be above the design S-N curve according to FAT 80, which can be concluded from Fig. 41 based on the solid finite element model. The last columns in Table 8 show the bending portion of the structural weld stress and the shear stress in the weld leg section, which is rather small so that the approach is applicable.

4.3.6 Application of the effective notch stress approach

Several computations with the effective notch stress approach were performed in a round robin for the IIW Guideline on this approach [12]. One representative analysis is described here, using the actual mean weld throat thicknesses given above [14].

The computation of the notch stresses was performed using the submodel technique. The coarse model shown in Fig. 42 was slightly refined in order to obtain improved prescribed displacements for the submodels. These were created with very fine meshes and subjected to prescribed deformations at the boundaries taken from the coarse model. Figure 45 shows typical submodels.

The weld root was modelled with a keyhole shape and a reference notch radius r_{ref}=1 mm. Eight-noded solid elements were chosen, having a length of about 0.1 mm at the notch.

To account for the different weld throat thicknesses given above, two models have been created. The computed fatigue notch factor K_f along the weld root line, related to the nominal stress in the RHS, is shown in Fig. 46 with a max. value K_f=9.03 for the axial load case and K_f=6.50 for the bending load case. The latter is decreased to K_f=5.97 if the throat thickness is increased to a=5.1 mm for the MAG-welded joints. The distribution differs slightly from that in Fig. 44.

Based on these factors, the fatigue lives are plotted in Fig. 47 in relation to the effective notch stress range. It can be seen that all test results are located above the S-N curve for the fatigue class FAT 225 according to the IIW Fatigue Design Recommendations [16]. Again, the values for bending are above those for axial loading as discussed in the previous sub-chapters.

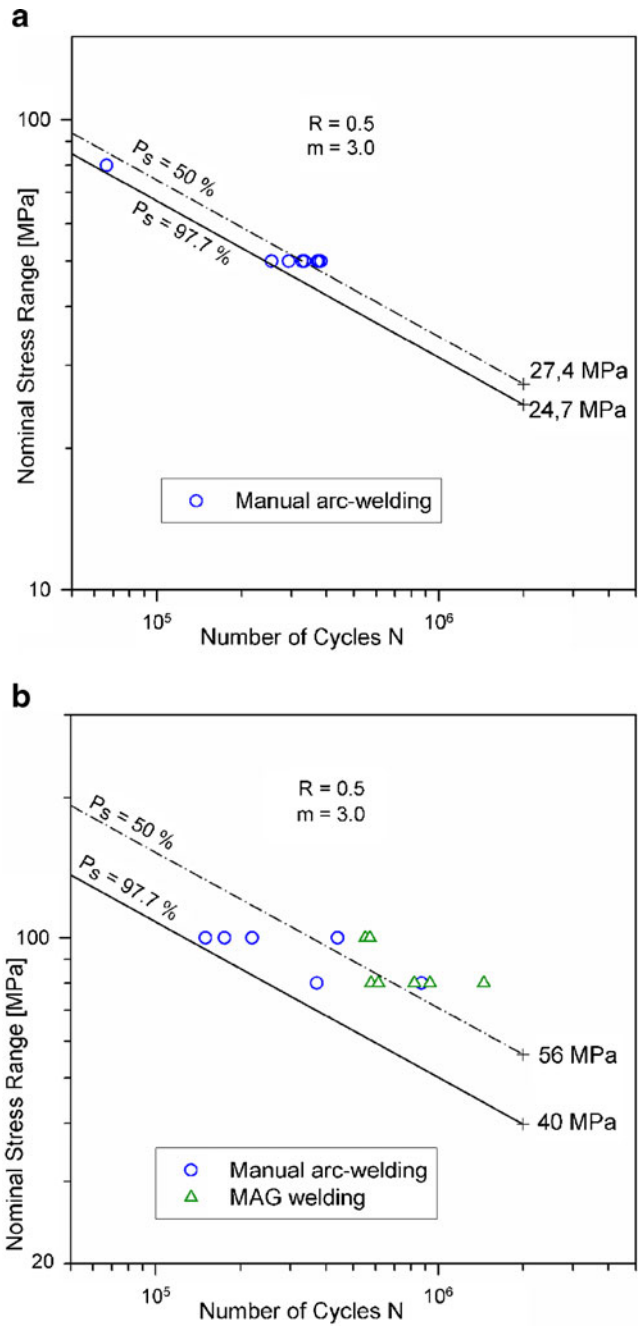

Fig. 41 Fatigue lives obtained for axial load **a** and bending load **b**

4.4 Lap joints and cover plates

4.4.1 Description of the detail

The fourth detail concerns test specimens of *lap joints* with an interrupted main plate and *cover plates* on a continuous main plate. In the first case, the fillet welds are full-load carrying, whereas those at cover plates are partial-load carrying, which has an effect on the local stresses at the weld toe and root. Figure 48 shows the geometry of the specimens. The arrangement of plates on both sides should avoid

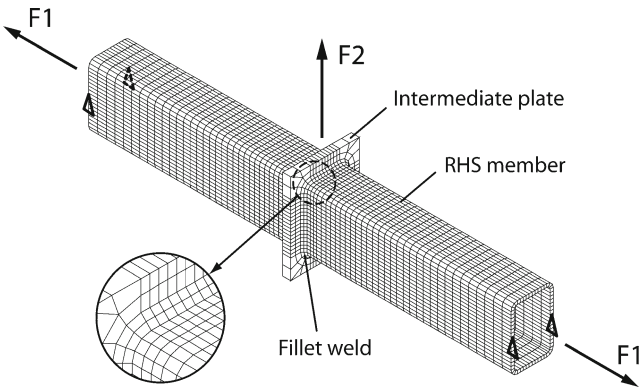

Fig. 42 Finite element model and loading of the RHS-joint

local bending. A plate thickness of 12 mm and two different weld throat thicknesses of a=3 and 7 mm were chosen, resulting in four different types of specimens, denoted L.3, L.7, C.3 and C.7.

The test specimens were fabricated from structural steel S355. While the fillet welds with a=3 mm were performed with one run, three runs were necessary for the throat thickness of 7 mm. The actual thickness varied between 2.9 and locally 5.0 mm and between 6.6 and 7.6 mm, respectively. In total, ten specimens were fabricated for each geometry. Further details are described by Fricke and Feltz [50].

4.4.2 Fatigue tests

The fatigue tests were performed with constant load amplitudes at different load levels, corresponding to nominal stress ranges in the plate in front of the weld between $\Delta\sigma_n$=90 and 210 N/mm^2. The stress ratio was $R\approx 0$.

Depending on the type of specimen, fatigue crack initiation was observed either at one of the weld toes, running through the main plate, or at one of the weld roots, propagating through the weld throat. Fracture of the specimen was taken as the failure criterion, as is usual for small-scale specimens. Mainly weld toe failures occurred, while weld root cracks were observed in all lap joints with a weld throat thickness a=3 mm (L.3) and three cover plates with the same weld throat thickness (C.3).

The fatigue lives of each test series were statistically evaluated assuming forced slope exponent m=3 for the S-N curves as typical for welded joints.

Table 7 Computed structural stress concentration factors $K_{s,w}$

Specimen type	Loading type	A (mm)	$K_{s,w}$
RHS, manual metal-arc welding	Axial	4.3	4.25
RHS, manual metal-arc welding	Bending	4.3	3.37
RHS, MAG-welded	Bending	5.1	2.78

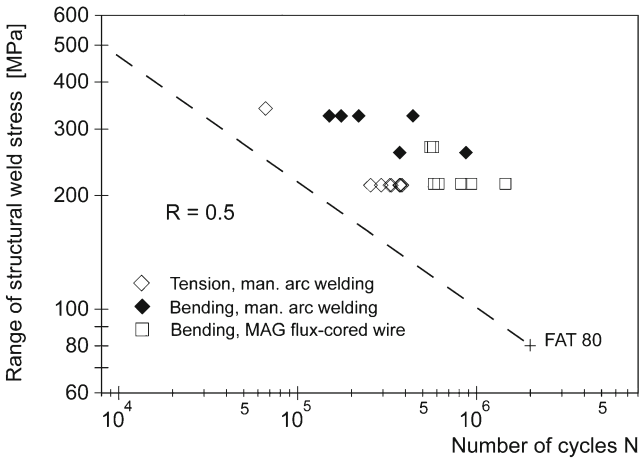

Fig. 43 S-N results of the fatigue tests using the computed range of structural weld stress

Figure 49 shows the fatigue lives of all specimens with weld toe failures. All results seem to fall into one scatter band. It is interesting to note that no difference is recognisable between lap joints (full-load carrying) and cover plates (partial-load carrying). The evaluated characteristic fatigue strength for a survival probability P_s=97.7 % at N=2·10^6 cycles is 78 N/mm^2.

The fatigue lives of the lap joints with throat thickness a=3 mm showing root failures (L.3) are summarised in Fig. 50. The statistical evaluation yields a characteristic fatigue strength of 40 N/mm^2. It should be borne in mind that the nominal stress is based on the main plate and that the weld stress is twice as high. The S-N curve seems to have a shallower slope causing a wide scatter band when m=3 is assumed.

4.4.3 Application of the nominal stress approach

The details investigated can be found in the catalogues of codes and recommendations based on the nominal stress approach. In case 611 of the IIW Fatigue Design Recommendations [16], the *lap joint* is classified as FAT 63 for weld toe failure (based on nominal stress in main plate) and FAT 45 for weld throat failure (based on nominal stress in weld throat). The above-mentioned test results are generally above these values, considering the difference between plate and weld stress.

The FAT value of the *cover plate* in the recommendations depends on the structural configuration. On a continuous plate, it is classified as FAT 71 (case 513), whereas on an I-beam or a rectangular hollow section, it corresponds to FAT 50 (cases 711 and 713). The first case agrees better with the test specimen because the latter includes additional structural stress concentrations. The test results are again on the safe side.

Table 8 Computed structural stress concentration factors $K_{s,w}$ and stress components

Specimen type	Loading type	a (mm)	$K_{s,w}$	(σ_b/σ_s)	(τ/σ_s) (%)
Manual metal-arc welding	Axial	4.3	3.92	79.8 %	0.55
Manual metal-arc welding	Bending	4.3	2.99	75.5 %	1.8
MAG-welded	Bending	5.1	2.54	75.7 %	1.9

4.4.4 Application of the effective notch stress approach

The effective notch stress approach, using the elastic stress in the notches rounded by a reference radius r_{ref}=1 mm, is able to assess both weld toes and weld roots. Relatively fine-meshed finite element models have been created for the numerical analyses (Fig. 51) using plane strain conditions and considering the recommendations [12]. The keyhole notch has been placed such that the minimum distance between the rounded notch surface and the weld surface is exactly the throat thickness (3 or 7 mm, respectively).

The analysis has been performed with contact elements between the main and lap/cover plates. A nominal stress of σ_n=150 N/mm^2 has been applied as typical for the tests.

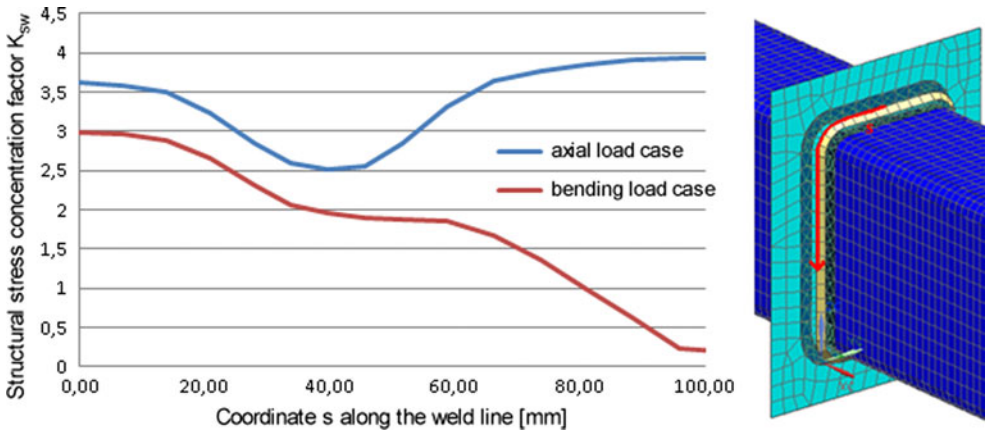

Fig. 44 Distribution of structural stress concentration factor K_{sw} along the weld line for a weld throat thickness a=4.3 mm

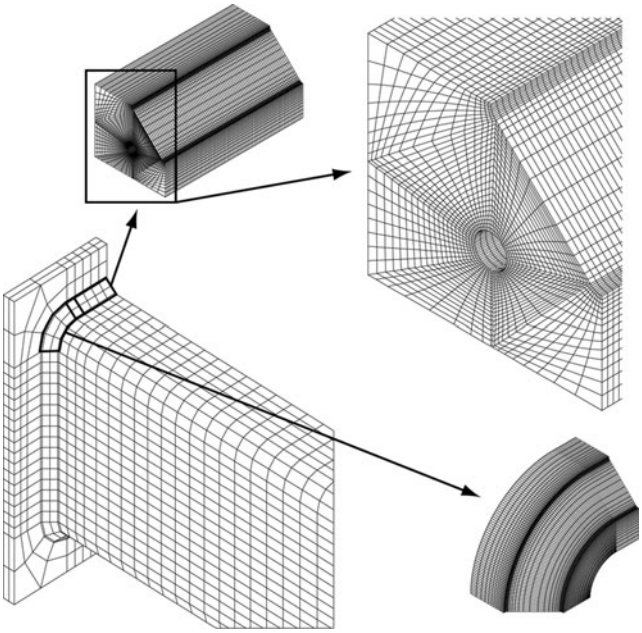

Fig. 45 Coarse finite element model and submodels for notch stress analysis

The resulting stress concentration factors, i.e. the max. principal stress in the notch related to the nominal stress, are given in Table 9. The expected failure location agrees with the tests only for two specimen types (L.3 and C.7). The notch stress at the weld root seems to be unrealistically high for the lap joint with a=7 mm (L.7). It can be stated that the effective notch stress is quite sensitive to the weld throat thickness, but also to the load carrying grade, particularly at the weld root.

Figure 52 shows the fatigue test data, using the effective notch stresses for the actual crack initiation site. It can be seen that the data are generally above the S-N curve according to FAT 225; however, the results for the root cracks are quite conservative which is obviously due to the increased stress concentration by the keyhole notch.

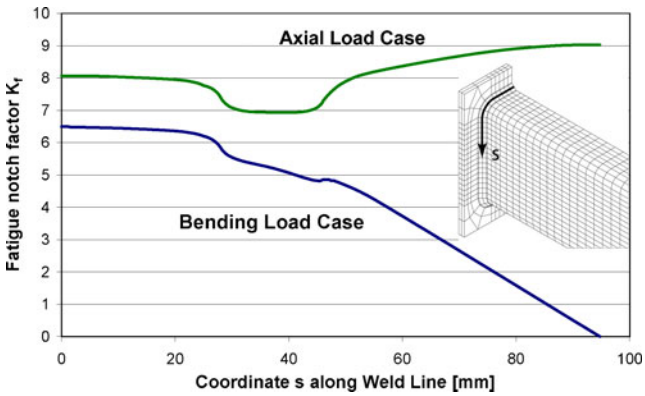

Fig. 46 Distribution of the fatigue notch factor along the weld root line for a weld throat thickness a=4.3 mm

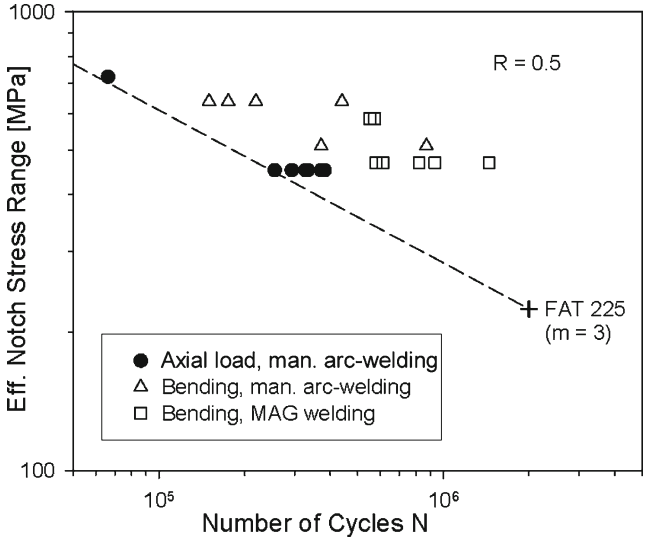

Fig. 47 S-N results of the fatigue tests using the computed range of effective notch stress

4.4.5 Application of the strain energy density approach

2D finite element models of the four types of specimens have been created, using plane strain elements with quadratic shape function. Contact elements were again applied to the slit between the main and lap/cover plates. Fine meshes as shown in Fig. 23 have been created where the average SED was determined for the control sector with R_0=0.28 mm using a subroutine in ANSYS [9]. In addition, relatively coarse meshes with an element length of $\ell = 0.28$ *and* $1.0\,mm$ at the notch tip were used. The SED of the latter has been converted from R^*=1 mm to R_0=0.28 mm. The computed range of the SED, $\Delta\overline{W}$, is given in Table 10 again for a nominal stress range $\Delta\sigma_n$=150 N/mm^2.

The difference between the coarse and fine meshes is small as long as the element length ℓ does not exceed 0.28 mm. For the coarse meshes with $\ell = 1\,mm$, the

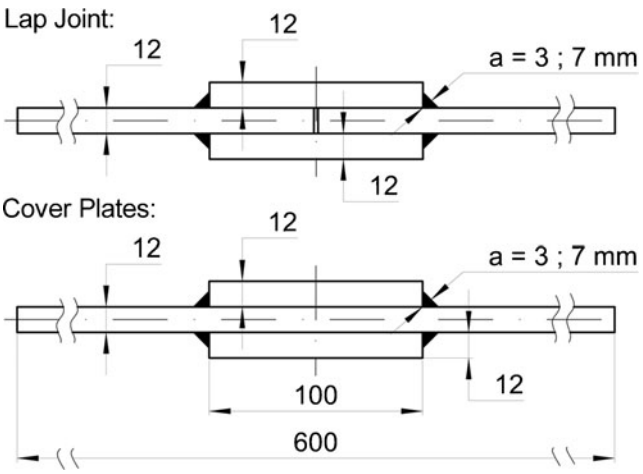

Fig. 48 Geometry of the lap joints and cover plates

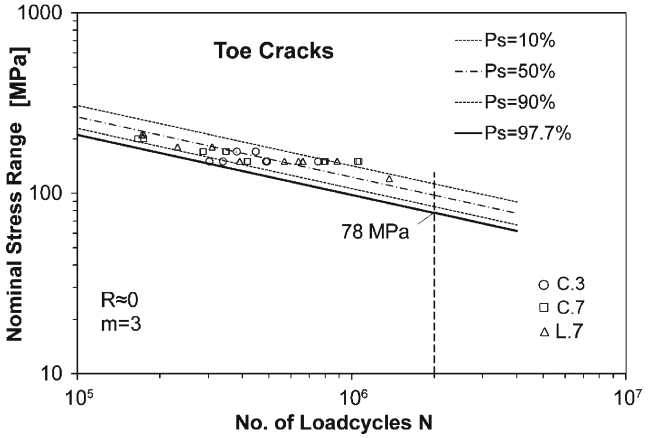

Fig. 49 S-N results for all specimens with weld toe failure

deviations are larger, but tolerable. At the weld root, the effect of the T-stress has been considered as described in Section 3 (Eq. 3.20).

The largest SED value at the toe or root determines the expected crack initiation site. It can be seen from Table 10 that the derived crack initiation site corresponds to the tests for three of the four types of specimens. The lap joint with a=7 mm (L.7) shows the highest SED at the weld root; however, fatigue cracks occurred at the weld toe. It should be mentioned that the SED at the weld root would be smaller if the control radius were R_0=0.36 mm instead of 0.28 mm. This would change the crack initiation site.

The average SED has been computed for different load levels because the contact creates a slightly non-linear response with increasing load. This allows plotting of the results in the S-N diagram in Fig. 53, here using the equivalent stress range according to Eq. (3.17) on the vertical axis instead of the SED. Also included is the scatter band according to the evaluation in Fig. 21, here in terms of the equivalent stress range.

Most of the results are within the scatter band except for the series L.3 failing from the weld root. The shallow slope

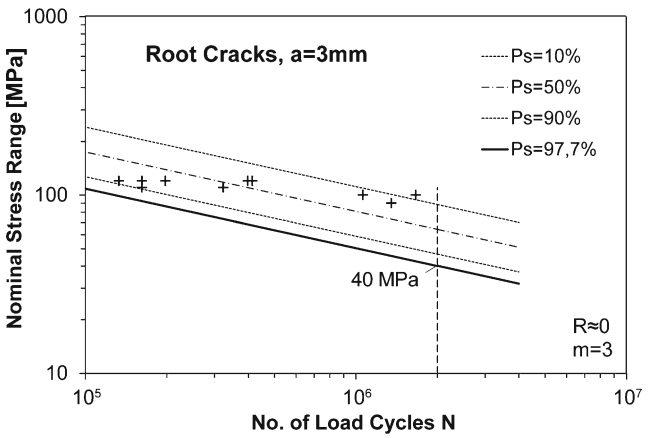

Fig. 50 S-N results for all L.3 specimens with weld root failure

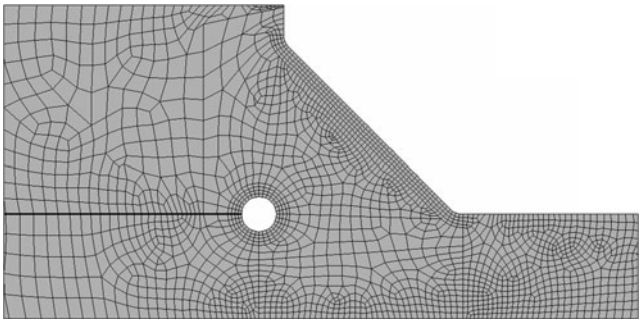

Fig. 51 Typical mesh (1/4 model) for effective notch stress analysis

of the S-N curve based on nominal stresses (Fig. 50) can also be recognised here. The results are on the safe side—as in the nominal and notch stress approaches.

4.4.6 Application of the crack propagation approach

The crack propagation analysis has been performed for all four types of specimens using the program FRANC2D [49] which applies the finite element method to the computation of the stress intensity factor (SIF). Using a relatively fine two-dimensional basic mesh, the area around the crack tip is re-meshed with appropriate fineness containing the crack. The SIF is calculated with the J integral method. This is performed for various crack lengths with given increment Δa, while the direction of crack propagation is determined by the SIFs for mode I and mode II. The finite element model in FRANC2D does not contain contact elements. Therefore, the contact between the main and cover or lap plates was realised by additional elements in the gap having usual axial stiffness, but negligible shear stiffness.

The fatigue life is determined using the computed SIFs and integrating the Paris–Erdogan law numerically from the initial to the final crack length. The initial crack length a_i has been assumed as 0.1 mm, whereas the final crack length has been set to approximately half plate thickness. The remaining life is neglected. The material parameters m=3 and C=5.21·10^{-13} (units, Newton and millimeters) recommended by Hobbacher [16] have been used, representing the upper limit of the scatter band (2.3 % probability of failure).

Table 9 Computed notch stress concentration factors for reference radius r_{ref}=1 mm (expected failure location highlighted)

Specimen type	K_f	
	At toe	At root
Lap joint a=3 mm	5.76	**7.34**
Cover plate a=3 mm	3.54	**3.60**
Lap joint a=7 mm	3.35	**4.12**
Cover plate a=7 mm	**2.82**	2.24

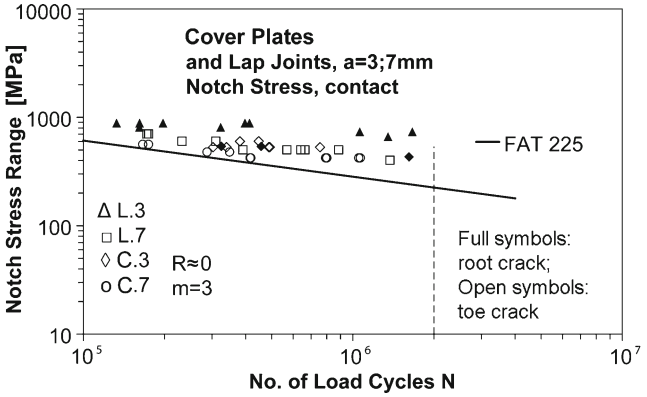

Fig. 52 S-N data based on effective notch stress

Figure 54 shows typical crack paths computed for the weld toe and the weld root. While the crack at the weld toe follows approximately the direction along half the notch opening angle, the direction is almost vertical at the weld root, which agrees with the observations in the tests at least in the middle part of the specimens.

The fatigue life (number of load cycles N) has been determined again with a nominal stress range $\Delta\sigma_n$=150 N/mm^2 in the main plate. From this, a characteristic fatigue strength $\Delta\sigma_c$ based on nominal stress was determined by extrapolating the result with a slope exponent m=3 to N=2·10^6. Table 11 summarises the results.

4.4.7 Comparison of all results on the basis of nominal stresses

The results from the different approaches can be compared on the basis of the characteristic fatigue strength at 2·10^6 cycles for a survival probability P_s=97.7 % based on nominal stress.

Table 12 summarises all computed characteristic fatigue strengths together with those derived from the tests. The relatively simple nominal stress approach is only partly able to identify the crack initiation site. The results for the thin welds (L.3 and C.3) show that the fatigue critical locations are generally quite well identified if the small difference between the values for the effective notch stress of C.3 is neglected. The same applies also to the cover plates with large weld throat thickness (C.7). Only the fatigue-critical location for the lap joint with thick welds (L.7; toe failure) is not well predicted. In the SED approach, this might be due to the too small control radius, whereas the results of the effective notch stress approach seem to be affected by the keyhole notch creating a too severe notch effect.

The crack propagation approach predicts the critical crack location very well, but the results are generally too low in comparison with those found in the tests (Figs. 49 and 50). A reason might be that the 2D analysis is rather conservative by assuming a continuous crack along the weld toe or root line, whereas the first part of crack propagation might be governed by semi-elliptical crack shapes, showing a reduced crack propagation rate. In contrast to the first example, semi-elliptical cracks are reasonable also for the weld root, where the slit is no longer perpendicular but parallel to the stresses. When assuming semi-elliptical crack shapes at both locations, the relation in fatigue lives between weld toe and weld root may remain unchanged.

4.5 Fillet-welded pipe penetration with multiaxial loading

4.5.1 Description of the detail

The fifth detail is a pipe penetration through a plate connected with fillet welds, see Fig. 55. The plate is subjected to axial nominal stress σ_n, creating a complex load situation in the weld. Weld root cracking is possible here, particularly at the 45° position, where radial stresses σ_r and shear stresses τ are transferred by the fillet welds. These stress components are to be determined and the weld stress superimposed according to Eq. (3.6).

Table 10 Computed $\Delta\overline{W}$ from different meshes for R_0=0.28 mm and $\Delta\sigma_n$=150 N/mm^2 (deviations in percentage refer to fine mesh results; expected failure location highlighted)

	$\Delta\overline{W}$ (Nmm/mm^3) for weld toe			$\Delta\overline{W}$ (Nmm/mm^3) for weld root[a]			
	Fine mesh (0.03 mm)	Coarse mesh (0.28 mm)	Coarse mesh (1 mm)	Fine mesh (0.03 mm)	Coarse mesh (0.28 mm)	Coarse mesh (1 mm)	σ_T[b] (MPa)
L.3	0.725	0.724 (0.2 %)	0.686 (5.4 %)	**1.107**	**1.089** (1.7 %)	**1.076** (2.8 %)	113
C.3	**0.352**	**0.352** (0.1 %)	**0.340** (3.4 %)	0.236	0.232 (1.6 %)	0.225 (4.5 %)	99
L.7	0.317	0.319 (0.7 %)	0.315 (0.4 %)	**0.393**	**0.395** (0.6 %)	**0.382** (2.9 %)	83
C.7	**0.241**	**0.244** (0.9 %)	**0.244** (1.1 %)	0.072	0.074 (2.3 %)	0.0678 (9 %)	83

[a] Smaller values would be obtained for R_0=0.36 mm

[b] T-stress used for the conversion of $\Delta\overline{W}$ from R=1 mm to R_0=0.28 mm

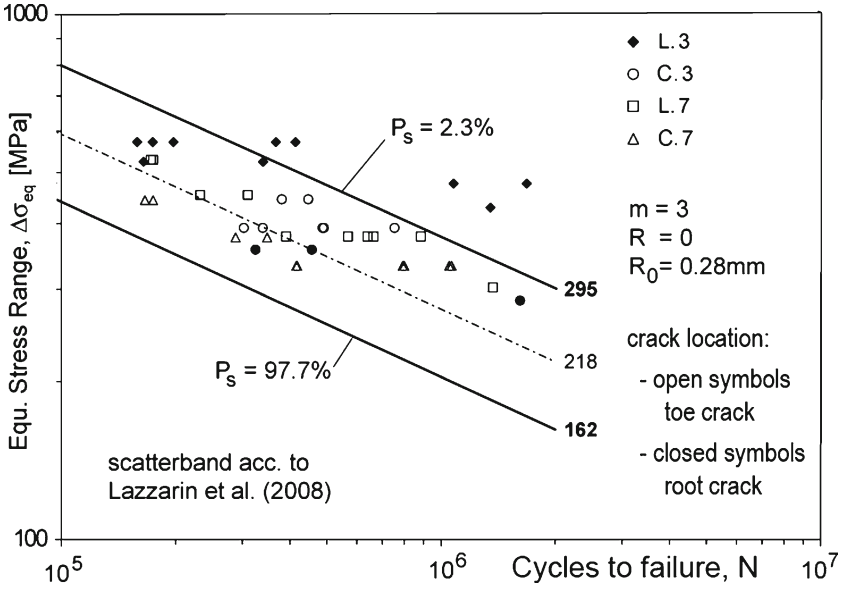

Fig. 53 S-N diagram showing the test results in terms of the equivalent stress

The data of the pipe penetration and loading are as follows:

Plate thickness	t_p=20 mm
Tubular thickness	t_r=30 mm
Mean radius	r=400 mm
Half height of tube	H=150 mm
Weld throat thickness	a=8 mm
Stress range in plate	$\Delta\sigma$=200 N/mm^2

4.5.2 Application of the nominal stress approach using stress concentration factors

The normal and shear stress ranges $\Delta\sigma_r$ and $\Delta\tau$ in the plate beside the weld can be determined using the design charts in [8]. These show the structural stress concentration factor K_s (there termed SCF) for these two stress components at different locations around the pipe as a function of the following geometry parameters:

t_r/t_p (=1.5)
r/t_p (=20)
H/t_r (=5)

Figure 56 shows the design charts for the normal and shear stresses at 45° for H/t_r=5, from which stress concentration factors K_s=0.325 and 0.75 can be read off, resulting in the following stress components in the plate:

$$\Delta\sigma_r = 65\mathrm{N}\Big/mm^2 \; and \; \Delta\tau = 150\mathrm{N}\Big/mm^2$$

The corresponding stresses in the weld can be calculated according to Fig. 9 as follows:

$$\Delta\sigma_\perp = \Delta\tau_\perp = \frac{\Delta\sigma_r \cdot t_p}{2a\sqrt{2}} = 57.4\mathrm{N}\Big/mm^2 \qquad (5.2)$$

$$\Delta\tau_{II} = \frac{\Delta\tau \cdot t_p}{2a} = 187.5\,\mathrm{N}\Big/mm^2 \qquad (5.3)$$

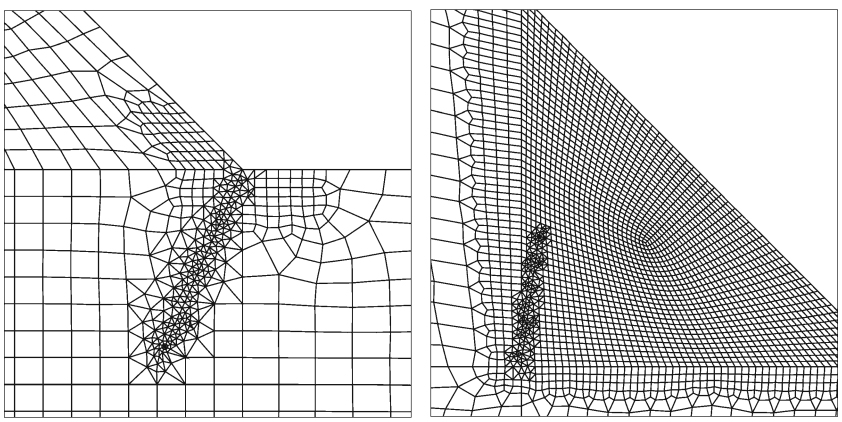

Fig. 54 Typical crack paths at the weld toe (*left*) and weld root (*right*)

Table 11 Computed fatigue life N from crack propagation approach for $\Delta\sigma_n$=150 N/mm^2 and derived characteristic fatigue strength $\Delta\sigma_c$ (expected failure location highlighted)

	Fatigue life N, crack at:		$\Delta\sigma_c$ (N/mm^2), crack at:	
	Weld toe	Weld root	Weld toe	Weld root
L.3	15,924	**7,112**	30.0	**22.9**
C.3	**40,835**	52,440	**41.0**	44.6
L.7	**49,313**	62,620	**43.5**	47.3
C.7	**67,513**	406,617	**48.5**	88.2

The following nominal weld stress results from Eq. (3.6):

$$\sigma_{n,w} = \sqrt{\sigma_\perp{}^2 + \tau_\perp{}^2 + 0.2{\cdot}\tau_{II}{}^2} = 116.7\,\mathrm{N}\Big/mm^2 \qquad (5.4)$$

The fatigue assessment can be performed on the basis of the fatigue class FAT 36 as $a>t_p/3$. Comparisons with different fatigue tests on similar geometries have shown the suitability of the procedure [51].

4.5.3 Application of the nominal stress approach using the finite element method

The model is created using shell elements in the way proposed in Fig. 14, with the geometrical parameters described above. The size of the plate is 5,000×5,000 mm (see Fig. 57) which can be assumed as infinite relative to the size of the tube. Tensile load corresponding to the nominal stress amplitude of 200 N/mm^2 is applied.

To evaluate the multiaxial nominal stresses in the weld, internal forces are extracted along the weld leg line. The nominal stress components in the weld $\Delta\sigma_\perp$, $\Delta\tau_\perp$ and $\Delta\tau_{II}$ are calculated directly from the forces using the weld throat thickness a. The three stress components and the resultant nominal weld stress $\Delta\sigma_{n,w}$ acc. to Eq. (3.6) for the angle of 45° are found as follows:

$$\Delta\sigma_\perp = 57.3\mathrm{N}\Big/mm^2;\ \Delta\tau_\perp = 72.3\mathrm{N}\Big/mm^2;$$
$$\Delta\tau_{II} = 168.6\mathrm{N}\Big/mm^2;\ \Delta\sigma_{n,w} = 119.2\mathrm{N}\Big/mm^2$$

The results are very close to the values in the previous section. The fatigue assessment is performed with the fatigue class FAT36 as mentioned before.

4.5.4 Application of the effective notch stress approach

The effective notch stress was computed with the fine-mesh finite element model shown in Fig. 58 representing 1/8 of the structure by utilising symmetry conditions of three planes including that at half plate thickness. The plate width chosen corresponds to ten times the pipe diameter in order to eliminate any boundary effects on the results.

Solid elements with quadratic shape function were applied. The weld root was idealised with a keyhole shape and element lengths down to 0.26 mm.

In the rounded notch surface at the 45° position, the nominal stress range $\Delta\sigma_n$=200 N/mm^2 creates the following principal stress components and equivalent von Mises stress range:

$$\Delta\sigma_1 = 740\ \mathrm{N}\Big/mm^2;\ \Delta\sigma_2 = -209\ \mathrm{N}\Big/mm^2;$$
$$\Delta\sigma_{eq} = 853.5\mathrm{N}\Big/mm^2$$

The results indicate that here we have a typical case with predominant shear stress, which is characterised by principal stresses with different signs, see Section 3.4.3. It is recommended to base the fatigue assessment on the equivalent von Mises stress together with a reduced fatigue class, i. e. FAT 200.

4.5.5 Comparison of the results

A comparison between all results can be performed on the basis of the characteristic fatigue strength $\Delta\sigma_c$ based on nominal stress, which can be derived from the assumed nominal stress, the computed local stress and the FAT class of the S-N curve. The results in Table 13 show some significant differences between the results. The relatively low fatigue strength obtained with the notch stress approach might be due to the thickness effect acting here.

Table 12 Characteristic fatigue strengths (Newtons per square millimeter) based on nominal stresses in main plate and m=3 (expected failure location highlighted)

Specimen type:	L.3		C.3		L.7		C.7	
Crack location:	Toe	Root	Toe	Root	Toe	Root	Toe	Root
Fatigue test (as-welded)	–	**40**	**78**	–	**78**	–	**78**	–
Nominal stress approach	63	**22.5**	**71**	–	63	**53**	**71**	–
Effect. notch stress approach	39.1	**30.7**	63.5	**62.5**	67.2	**54.6**	**79.8**	100.4
SED approach[a]	42.4	**34.3**	**60.9**	74.4	64.2	**57.6**	**73.5**	134.6
Crack propagation approach	30.0	**22.9**	**41.0**	44.6	**43.5**	47.3	**48.5**	88.2

[a] Computed with R_0=0.28 mm

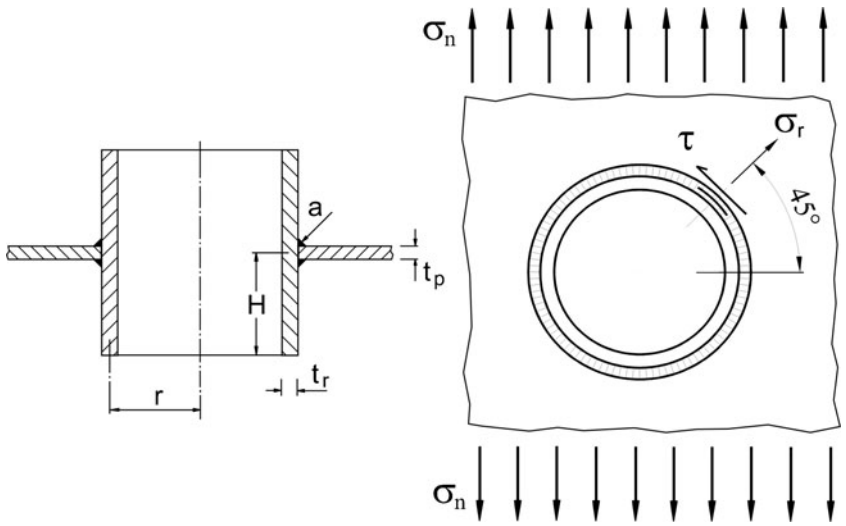

Fig. 55 Geometry of the pipe penetration and location of the point considered

4.6 Laser-stake welded T-joint

4.6.1 Description of the detail

The investigation of laser-stake welded T-joints was reported by Frank et al. [10], where 8-mm-thick plates were used in three of four series. Figure 59 shows the geometry. The web plate of the joint was subjected to cyclic tensile stress $\Delta\sigma_n$, while the face plate was clamped by bolts. Fatigue cracks occurred at the laser-welded connection between web and face plates.

The S-N curve derived from all fatigue tests shows a mean fatigue strength of 48 N/mm^2 at $2{\cdot}10^6$ load cycles and a slope exponent of m=4.5. If a typical scatter ratio of T_σ=1:1.5 between 90 and 10 % probability of survival is assumed, the characteristic fatigue strength at $2{\cdot}10^6$ load cycles becomes 35 N/mm^2 for a survival probability P_s=97.7 %.

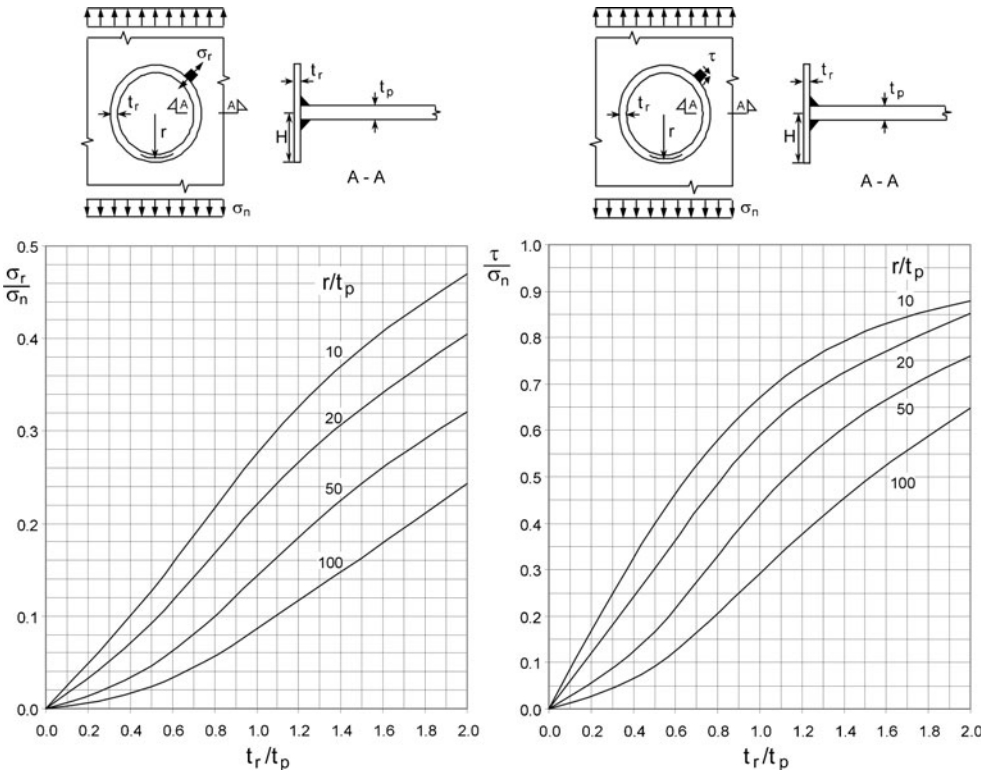

Fig. 56 Design charts for normal and shear stress in the plate at 45° for H/t_r=5 [8]

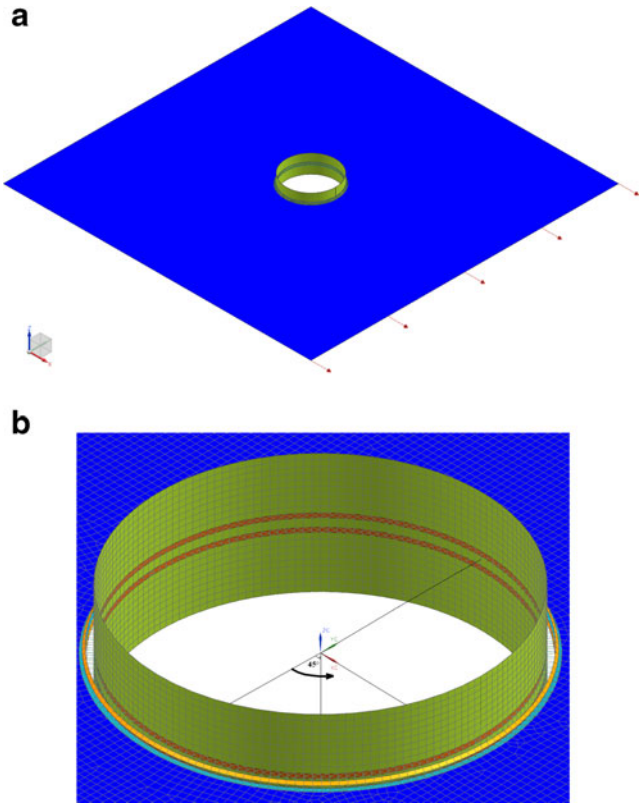

Fig. 57 Finite element model and angle definition

Nominal weld stress and local stresses are determined for the following geometry, which is close to the average of the first three test series mentioned:

Face plate thickness	t_f=8 mm
Web thickness	t_w=8 mm
Width of face plate	b_f=20 mm (between clamping points)
Height of web	h_w=50 mm
Width of the weld	t_{weld}=3 mm
Weld eccentricity	e_{weld}=0.3 mm
Width of root face at left	a_1=2.8 mm
Width of root face at right	a_2=2.2 mm

Table 13 Characteristic nominal fatigue strength derived from the approaches

Characteristic fatigue strength $\Delta\sigma_c$ based on nominal stress, derived from	
Nominal stress approach	Effective notch stress approach
60.4–61.7 N/mm^2	46.9 N/mm^2

The nominal stress range is set to $\Delta\sigma_n$=35 N/mm^2, corresponding to the characteristic fatigue strength at $2{\cdot}10^6$ cycles in the tests. A 2D model with plane strain conditions is analysed. Boundary conditions are included in Fig. 59.

4.6.2 Application of the nominal stress approach

In the nominal stress approach, the nominal weld stress $\Delta\sigma_{n,w}$ is used. This is simply determined by referring the nominal stress in the web to the weld throat area, resulting in:

$$\Delta\sigma_{n,w} = \Delta\sigma_n \cdot t_w \Big/ t_{weld} = 93\ \mathrm{N}\Big/mm^2 \tag{5.5}$$

This value is far above the relevant fatigue class FAT 36, resulting in a fatigue life of 116,000 load cycles if the slope exponent m=3 is used, so that the fatigue assessment would be quite conservative compared with the tests.

4.6.3 Application of the effective notch stress approach

The effective notch stress approach with reference radii r_{ref}=1 mm and r_{ref}=0.05 mm has been applied, although the latter is not explicitly recommended for plate thicknesses of 5 mm and more. However, the weld thickness is rather small. The numerical analysis is performed with two FE models shown in Fig. 60. These models are generated in accordance with the recommendations in Section 3.4.2 and in [12] using higher-order 2D elements with eight nodes each. The keyhole notches are positioned in such a way that

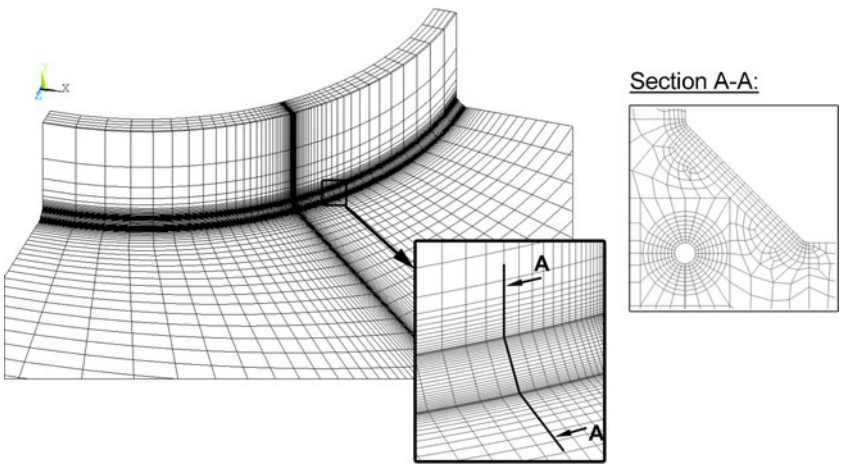

Fig. 58 Finite element model of the pipe penetration for the application of the effective notch stress approach

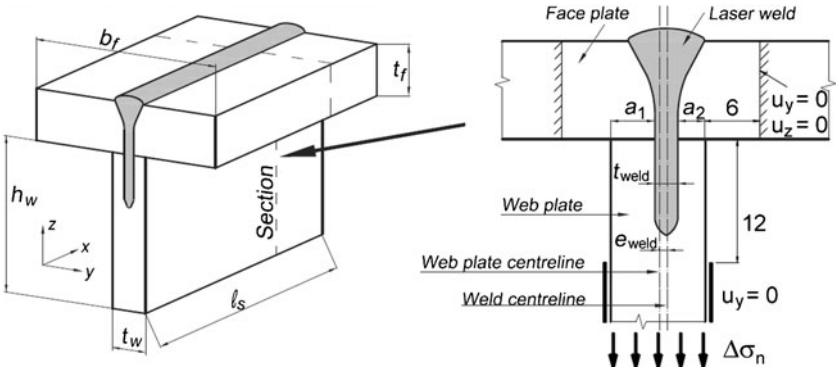

Fig. 59 Geometry, loading and boundary conditions of the laser-stake welded T-joint

the weld thickness t_{weld}=3 mm is kept between the vertex points of the keyhole notches.

The effective notch stress is defined as the maximum principal stress at the edge of the keyhole notches. The right notch with the smaller non-fused root face turned out to have the higher notch stress. Results are given in Table 14.

Assuming design S-N curves according to Table 1, with FAT 225 for r_{ref}=1 mm and FAT 630 for r_{ref}=0.05 mm, the computed fatigue lives in Table 14 show that the first approach is non-conservative, whereas the latter is conservative at least in the given nominal stress range, being the characteristic value of the tests for two million cycles.

4.6.4 Application of the strain energy density approach

To calculate the SED $\Delta\overline{W}$, another two-dimensional plane strain FE model is created which includes two control areas spanned by the radii R_0=0.28 mm around the notch tips as seen in Fig. 61.

Within the control areas, six elements are arranged along the radius R_0 which results in an element length of $\ell \approx 0.047\,mm$. The calculated range of the SED in the right notch is $\Delta\overline{W} = 0.0453\,Nmm/mm^3$ for the nominal stress range $\Delta\sigma_n$=35 N/mm^2. This SED is slightly below the characteristic value given in Fig. 21 so that the approach is unconservative in this load range.

Formula (3.16) can be used to obtain the stress intensity factor range ΔK_1. When only mode 1 is observed this equation results in

$$\Delta K_1 = \sqrt{\frac{\Delta\overline{W}\cdot E}{e_1}}\cdot R_0^{1-\lambda_1} \tag{5.6}$$

For the present calculation, the notch opening angle is α=0°; thus, the following parameters are used in accordance with Table 2: e_1=0.133 and eigenvalue of stress field for

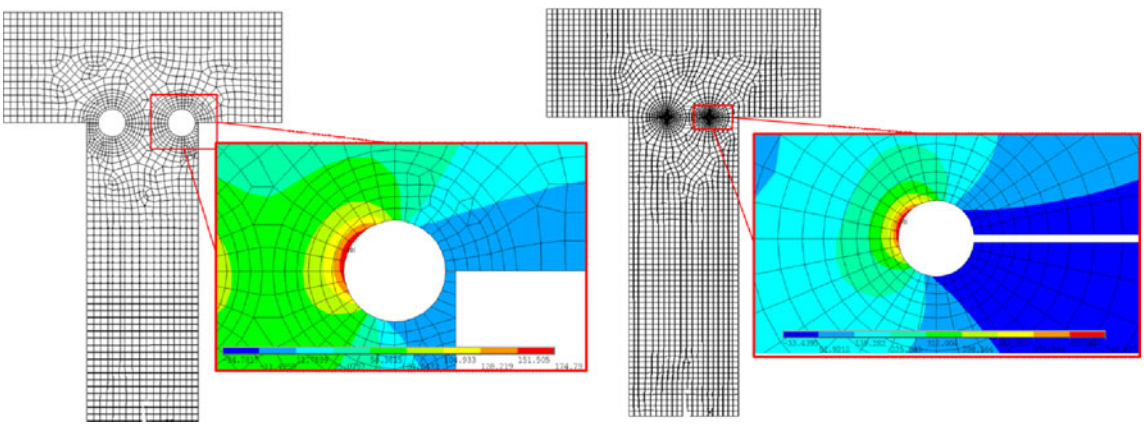

Fig. 60 Typical mesh for effective notch stress analysis with reference radius r_{ref}=1 mm (*left*) and r_{ref}=0.05 mm (*right*) and max. principal stress distribution

Table 14 Computed effective notch stresses, stress concentration factors and fatigue lives for nominal stress $\Delta\sigma_n$=35 N/mm^2 and reference radii r_{ref}=1 mm and r_{ref}=0.05 mm

Reference radius r_{ref} (mm)	Effective notch stress (N/mm^2)	Stress concentration factor K_f	Fatigue life N for $\Delta\sigma_n$=35 N/mm^2
1	174.8	4.99	3,291,000
0.05	743.8	21.25	938,000

mode 1 λ_I=0.5. The range of the stress intensity factor becomes ΔK_1=140.9 N/mm$^{3/2}$.

4.6.5 Application of the crack propagation approach

The numerical analysis of the stress intensity factors was performed with the program FRANC2D [49]. Figure 62 shows the two-dimensional finite element mesh with eight-node plane strain elements and the finer re-meshed area around the crack path. The initial crack length was set to a_i=0.07 mm (in addition to the non-fused root face a_2=2.2 mm). The final crack length was a_f=3.02 mm corresponding to the weld thickness, see Fig. 62.

The number of load cycles during crack propagation is estimated by the Paris–Erdogan equation (3.21), again with material parameters C=5.21 10^{-13} (Newton, millimeters) and m=3 according to [16]. The calculation was performed with a crack length increment da=0.05 mm. The final crack length was reached at N=0.88·10^6 load cycles which is below the characteristic load cycle number N_c=2·10^6. Thus, the crack propagation approach is conservative at least in the given load range.

4.6.6 Comparison of the results

Table 15 compares the fatigue lives computed and observed in the tests, based on P_s=97.7 %. The differences are quite large. The crack propagation approach yields the best result.

5 Summary

Weld root fatigue can be a problem particularly for welds without full penetration, as the slit between non-welded root faces acts like an initial crack. Several approaches exist for the fatigue assessment of weld roots which have been summarised in Chapter 3 of this Guideline. In addition to the nominal stress approach, which simply utilises an averaged stress in the weld throat, the structural stress approach may be applied, e.g. to consider increased stresses or bending in the weld throat. The effective notch stress and the notch stress intensity approaches also consider a single relevant parameter, i.e. a local stress, whereas the crack propagation approach uses the stress intensity factor computed for a growing crack.

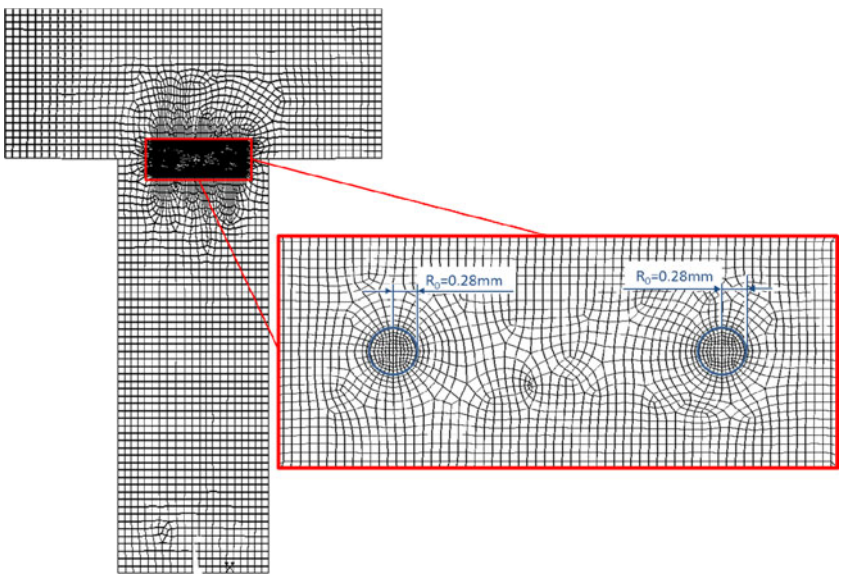

Fig. 61 FE model for the computation of the SED and control radii R_0=0.28 mm in finer-meshed area

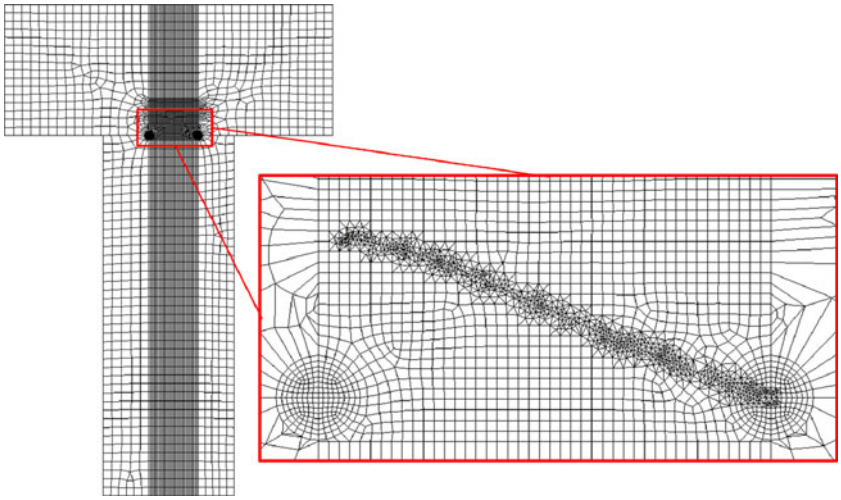

Fig. 62 Typical mesh for the crack propagation approach and crack path in refined mesh area

Table 15 Fatigue life N of the laser-stake welded T-joint from different approaches

Analysis method	Test	Nominal stress approach	Effective notch stress approach	SED approach	Crack propagation approach
No. of load cycles N	2,000,000	116,000	3,290,000	2,900,000	880,000

The different approaches have been applied to six examples which were partly fatigue tested so that a comparison with experiments is possible. The examples include the following details:

- Cruciform joints
- Fillet weld around attachment end
- One-sided fillet weld around RHS joint
- Lap joint and cover plates
- Fillet-welded pipe penetration
- Laser-stake welded T-joint

Two to four approaches have been applied to each detail so that the suitability of the approaches for the different details can be assessed. Corresponding comments have been given.

Acknowledgments The document is a product of several years of study by Working Group 3, 'Stress Analysis' of IIW Commission XIII. The support by the Chairmen of Commission XIII, Prof. G. Marquis (Finland), and Commission XV, R.E. Shaw (USA), and of the Joint Working Group of Commissions XIII/XV, A. Hobbacher (Germany) is appreciated. Special acknowledgement is made to all members of the working group for their review and valuable discussions and in particular to the following for thier contributions to the text and demonstration examples: J. Baumgartner, C. Fischer, C. Robert and C.M. Sonsino from Germany, I. Lotsberg from Norway, Z. Barsoum from Sweden, G. Meneghetti from Italy, H. Remes from Finland and D. Turlier and F. Menan from France.

References

1. Andrews R M (1988) The effect of misalignment on the fatigue strength of welded cruciform joints. IIW-Doc. XIII-1180-85
2. Anderson TL (1995) Fracture mechanics: fundamentals and applications, 2nd edn. CRC Press, Boca Raton
3. Barsoum Z, Barsoum I (2009) Residual stress effects on fatigue life of welded structures using LEFM. Eng Fail Anal 16:449–467
4. Barsoum Z (2008) Residual stress analysis and fatigue of multi-pass welded tubular structures. Eng Fail Anal 15:863–874
5. Boukharouba T, Tamine T, Nui L, Chehimi C, Pluvinage G (1995) The use of notch stress intensity factor as a fatigue crack initiation parameter. Engng Fract Mech 52:503–512
6. BS 7608 (1993) Code of practice for fatigue assessment of steel structures. British Standards Institution, London
7. Carpinteri A (ed) (1994) Handbook of fatigue crack propagation in metallic structures. Elsevier, Amsterdam
8. DNV (2010) Fatigue strength analysis of offshore steel structures. Report DNV-RP-C203, Det Norske Veritas, Høvik
9. Fischer C, Feltz O, Fricke W, Lazzarin P (2011) Application of the notch stress intensity and crack propagation approaches to weld toe and root fatigue. Weld World 50(7/8):30–39
10. Frank D, Remes H, Romanoff J (2011) Fatigue assessment of laser stake-welded joints. Int J Fatigue 33:102–114
11. Fricke W (2005) Effects of residual stresses on the fatigue behaviour of welded steel structures. Mat-wiss u Werkstofftech 36:642–649
12. Fricke W (2012) IIW recommendations for the fatigue assessment of welded structures by notch stress analysis. Woodhead Publishing, Cambridge
13. Fricke W, Doerk O (2006) Simplified approach to fatigue strength assessment of fillet-welded attachment ends. Int J Fatigue 28:141–150
14. Fricke W and Kahl A (2006). Fatigue assessment of weld root failure of hollow section joints by structural and notch stress approaches. In: Proc of In. Symp on Tubular Structures (ISTS'11), Quebec
15. Fricke W, Kahl A and Paetzold H (2006) Fatigue assessment of root cracking of fillet welds subject to throat bending using the structural stress approach. Weld World 50(7/8):64–74
16. Hobbacher A (2009) *Recommendations for Fatigue Design of Welded Joints and Components*. IIW doc.1823-07, Welding Research Council Bulletin 520, New York

17. Hong J K (2010): Evaluation of weld root failure using Batelle structural stress method. In: Proc. 29th Int Conf on Ocean, Offshore & Arctic Engng (OMAE2010). ASME, New York
18. Lazzarin P, Tovo R (1998) A notch intensity factor approach to the stress intensity of welds. Fatig Fract Eng Mater Struct 21:1089–1103
19. Lazzarin P, Zambardi R (2001) A finite-volume-energy-based approach to predict the static and fatigue behaviour of components with sharp V-shaped notches. Int J Fracture 112:275–298
20. Lazzarin P, Berto F, Gomez FJ, Zappalorto M (2008) Some advantages derived from the use of the strain energy density over a control volume in fatigue strength assessments of welded joints. Int J Fatigue 30:1345–1357
21. Lazzarin P, Meneghetti G, Berto F and Zappalorto M (2009) Practical application of the N-SIF approach in fatigue strength assessment of welded joints. Weld World 53(3/4):R76–R89
22. Livieri P, Lazzarin P (2005) Fatigue strength of steel and aluminium welded joints based on generalized stress intensity factors and local strain energy values. Int J Fract 133:247–278
23. Lotsberg I (2003) Fatigue capacity of fillet welded connections subjected to axial and shear loading. IIW-Doc. XIII-2000-03/XV-1146-03
24. Maddox S.J (1974) Assessing the significance of flaws in welds subject to fatigue. Welding J., Res. Suppl. 53:9, pp. 401s–409s
25. Maddox S J and Razmjoo G R (1998): Fatigue Performance of Large Girth Welded Steel Tubes. In: Proc. 17th Int. Conf. Offshore Mechanics and Arctic Engng. (OMAE'98). ASME, New York
26. Maddox S J, Doré M J and Smith S D (2010) Investigation of ultrasonic peening for upgrading a welded steel structure. IIW-Doc. XIII-2326-10
27. Meneghetti G, Lazzarin P (2006) Significance of the elastic peak stress evaluated by FE analyses at the point of singularity of sharp V-notched components. Fatig Fract Eng Mater Struct 30:95–106
28. Meneghetti G (2008) The peak stress method applied to fatigue assessments of steel and aluminium fillet welded joints subjected to mode-I loading. Fatig Fract Eng Mater Struct 31(5):346–369
29. Meneghetti G and Lazzarin P (2011) The peak stress method for fatigue strength assessments of welded joints with weld toe and weld root failures. Weld World 55(7/8):22–29
30. Niemi E, Fricke W, Maddox SJ (2006) Fatigue analysis of welded components—designer's guide to the hot-spot stress approach. Woodhead Publishing, Cambridge
31. Radaj D, Sonsino C M and Fricke W (2006) Fatigue assessment of welded joints by local approaches, 2nd edn. Woodhead Publishing, Abington
32. Radaj D, Lazzarin P, Berto F (2009) Fatigue assessment of welded joints under slit-parallel loading based on strain energy density or notch rounding. Int J Fatigue 31:1490–1504
33. Schijve J (2001) Fatigue of structures and materials. Kluwer Academic, Dordrecht
34. Sonsino CM (2009) Effect of residual stresses on the fatigue behaviour of welded joints depending on loading conditions and weld geometry. Int J Fatigue 31(1):88–101
35. Sonsino C M (2009b) A consideration of allowable equivalent stresses for fatigue design of welded joints according to the notch stress concept with reference radii r_{ref}=1.00 and 0.05 mm. Welding in the World 53(3/4):R64–R75
36. Sonsino CM (2009) Multiaxial fatigue assessment of welded joints—recommendations for design codes. Int J Fatigue 31:173–187
37. Sonsino, C M (2011) Reliability aspects in fatigue design of welded structures using selected local approaches: the example of K-nodes for offshore constructions. In: K A McDonald (ed) Fracture and fatigue of welded joints and structures. Woodhead Publishing, Cambridge, pp. 239–275.
38. Sonsino CM, Bruder T, Baumgartner J (2010) S–N lines for welded thin joints—suggested slopes and FAT values for applying the notch stress concept with various reference radii. Weld World 54(11/12):R375–R392
39. Sonsino C M and Wiebesiek J (2007) Assessment of multiaxial spectrum loading of welded steel and aluminium joints by modified equivalent stress. IIW-Doc. XIII-2158r1-07/XV-1250r1-07
40. Sørensen J D, Tychen J, Andersen J U and Brandstrup R D (2005) Fatigue analysis of load-carrying fillet welds. In: Proc Int Conf on Offshore Mechanics and Arctic Engng (*OMAE'05*), OMAE-05-1006. ASME, New York
41. Tovo R, Lazzarin P (1999) Relationship between local and structural stress in the evaluation of the weld toe stress distribution. Int J Fatigue 21:1063–1078
42. Turlier D, Klein P and Bérard F (2010): "Seam Sim" method for seam weld structural assessment within a global structure FEA. In: Proc. Int. Conf. IIW2010 Istanbul (Turkey). AWST, pp. 651–658.
43. Turlier D, Klein P, De Noni L, Lawrjaniec D (2011) New FEA shell element model for seam weld static and fatigue structural assessment. In: Proc. Int. Conf. Fatigue Design 2011 (CETIM).
44. Verreman Y, Nie B (1996) Early development of fatigue cracking at manual fillet welds. Fatig Fract Eng Mater Struct 19:664–681
45. Wiebesiek J and Sonsino C M (2010) New Results in multiaxial fatigue of welded aluminium joints. IIW-Doc. XIII-2314-10/XV-1349-10
46. Williams M (1952) Stress singularities resulting from various boundary conditions in angular corners of plates in extension. J Appl Mech 19:526–528
47. Williams M (1957) On the stress distribution at the base of a stationary crack. J Appl Mech 24:109–114
48. Xiao ZG, Yamada K (2004) Fatigue strength evaluation of root failed joints on one millimeter stress. J Struct Eng 50A(2):719–726
49. Franc2D/L (2004): http://www.cfg.cornell.edu/software/franc2d_casca.htm
50. Fricke W, Feltz O (2010) Fatigue tests and numerical analyses of partial-load and full-load carrying fillet welds at cover plates and lap joints. Weld World 54(7/8):R225–R233
51. Lotsberg I (2004) Fatigue design of welded pipe penetrations in plated structures. Mar Struct 17:29–51